

POLITECNICO
MILANO 1863

Facoltà di Ingegneria Industriale
Dipartimento di Scienze e Tecnologie Aerospaziali
Corso di Laurea Magistrale in Ingegneria Aeronautica

# DNS of a turbulent channel flow over a rough wall

*Relatore:* Maurizio Quadrio

*Tesi di Laurea di:*
Michele Pinelli
Matricola: 833981

*Anno Accademico: 2016 - 2017*

**Abstract**

We develop a Direct Numerical Simulation (DNS) code for a turbulent open channel flow over a rough wall, in order to model the behaviour of the water-stream on a river bed. The purpose of this research is to create a DNS code suitable for the comparison with other less expensive simulations (RANS or LES for example) to determine their effectiveness on the case described above. In the fluid region the flow is governed by the Navier-Stokes equations, while the rough bottom is modelled by spheres thanks to the Immersed Boundary Method (IBM). In order to develop the final code we will make small steps, increasing the complexity of the flow for each of them. We start from the easiest case, a laminar $2D$ channel flow, and we will end with the channel flow with a rough wall, adding 9216 spheres over the bottom surface. The solid particles are not moving and are stuck on the bottom. The DNS solver used to integrate the equations is the University of California Irvine's solver, usually used for multiphase Homogenous Isotropic Turbulence. These governing equations are discretized in space in an Eularian framework using a second-order finite-difference scheme on a uniform staggered mesh, while the time integration is performed via the Adams–Bashforth scond-order scheme. The friction Reynolds Numbers chosen for all of the DNSs are around 180, because it is the same used in the validation papers. For all of the turbulent flows we analyze the turbulence statistics and the flow fields. For every case studied we compare the results with different papers in order to validate them. In the end we compare the two open channel flows, the smooth one and the one with the spheres on the bottom, to define if the behaviour found by our code is correct compared to the one found by Chan-Braun et al. [8]. From these last comparisons we are able to determine the influence of the rough bottom on a turbulent flow with a constant Reynolds Number.

# List of Figures


1.1 Theoretical law of the wall in viscous and logarithmic region . . . 15
1.2 Definition of $\Delta u^+$ in order to describe the difference between a flow over a rough and a smooth wall in the law of the wall . . . . 16
1.3 Instantaneous passive scalar contours superimposed on mean streamlines. From top to bottom, $\frac{w}{k} = 0.5, 1, 3, 7$. From Leonardi et al. [19] study. . . . . 17

2.1 Sketch of the channel flow . . . . . 22

3.1 Shear stresses non-dimensionalized by $Re_\tau$ with the y grid-size of Kim et al. [14] for channel flow . . . . . 32
3.2 Comparison of the mean velocity over horizontal planes in the homogenous direction and time with the y grid-size of Kim et al.[14] for channel flow . . . . . 33
3.3 Comparison of the mean velocity over horizontal planes in the homogenous direction and time with the y grid-size of Kim et al. [14] with semilogarithmic axes for channel flow . . . . . 34
3.4 Shear stresses non-dimensionalized by $Re_\tau$ with double of the y grid-size of Kim et al. [14] for channel flow . . . . . 35
3.5 Comparison of the mean velocity over horizontal planes in the homogenous direction and time with double of the y grid-size of Kim et al. [14] for channel flow . . . . . 36
3.6 Comparison of the mean velocity over horizontal planes in the homogenous direction and time with double of the y grid-size ofKim et al. [14] with semilgarithmic axes for channel flow . . . . 37
3.7 Comparison of the mean velocity over horizontal planes in the homogenous direction and time with half of the y grid-size of Chan-Braun et al. [8] with semilgarithmic axes for open channel (CPG) . . . . . 38
3.8 Comparison of the mean velocity over horizontal planes in the homogenous direction and time with the y grid-size of Chan-Braun et al. [8] with semilogarithmic axes for open channel flow (CPG) . . . . . 39
3.9 Comparison of the mean velocity over horizontal planes in the homogenous direction and time with half of the y grid-size of Chan-Braun et al. [8] for open channel (CFR) . . . . . 40

3.10 Comparison of the mean velocity over horizontal planes in the homogenous direction and time with half of the y grid-size of Chan-Braun et al. [8] with semilgarithmic axes for open channel (CFR) . . . . . 41

4.1 1 x 1 domain with the distribution of spheres . . . . . 45
4.2 Comparison of the mean velocity over horizontal planes in the homogenous direction and time with one eight of the grid-size of Chan-Braun et al. [8] for an open channel flow over a rough wall 47
4.3 Comparison of the mean velocity over horizontal planes in the homogenous direction and time with one eight of the grid-size of Chan-Braun et al. [8] with semilogarithmic axes for an open channel flow over a rough wall . . . . . 48
4.4 Comparison of the first three components of the Reynolds stresses with one eight of the grid-size of Chan-Braun et al. [8] . . . . . 49
4.5 Comparison of the mean velocity over horizontal planes in the homogenous direction and time with the grid-size of Chan-Braun et al. [8] for an open channel flow over a rough wall . . . . . 50
4.6 Comparison of the mean velocity over horizontal planes in the homogenous direction and time with the grid-size of Chan-Braun et al. [8] with semilogarithmic axes for an open channel flow over a rough wall . . . . . 51
4.7 Comparison of the first three components of the Reynolds stresses with the grid-size of Chan-Braun et al. [8] . . . . . 52
4.8 Comparison between rough and smooth wall theoretical curves and the results of our DNS . . . . . 54
4.9 Comparison between the results we have from our code and the ones found by Chan-Braun et al [8] . . . . . 55
4.10 Roughness function for several transitionally rough surface as a function of the Reynolds number based on $k_\infty^+$ from several paper. Picture taken from Chan-Braun et al. [8]. . . . . 55

# List of Tables

3.1 Comparison between the friction coefficients found by our code e by Kim et al. [14] for the coarser grid-size case . . . . . 31
3.2 Comparison between the friction coefficients found by our code e by Kim et al. [14] for the finer grid-size case . . . . . 31

4.1 Comparison between the difference in the viscous velocity due to the roughness found by Chan-Braun et al [8] and our code . . . . 54

# Contents

**Introduction** **9**

**1 Flows over rough walls** **13**
1.1 Physical problem . . . . . 13
1.2 Law of the wall . . . . . 14
1.3 Roughness . . . . . 16
1.4 Experimental researches . . . . . 18
1.5 Numerical researches . . . . . 19
1.6 Present work . . . . . 20

**2 Description of the method** **21**
2.1 Channel flow . . . . . 21
2.1.1 Boundary conditions . . . . . 21
2.2 Open channel flow . . . . . 22
2.2.1 Boundary conditions . . . . . 22
2.3 Governing equations . . . . . 23
2.3.1 Forcing term . . . . . 23
2.4 Numerical method . . . . . 26
2.4.1 Immersed Boundary Method . . . . . 26

**3 Validation for the smooth channel flows** **29**
3.1 Channel flow . . . . . 29
3.1.1 Comparison . . . . . 30
3.2 Open channel flow . . . . . 32
3.2.1 Constant Pressure Gradient . . . . . 32
3.2.2 Constant Flow Rate . . . . . 38

**4 Channel flow with roughness** **43**
4.1 Description of the geometry . . . . . 43
4.2 Comparison . . . . . 44
4.3 Law of the wall . . . . . 53

**5 Conclusions and future work** **57**

**Appendix** **59**
A.1 Initial Conditions . . . . . 59
A.2 Post Processing . . . . . 59

# Introduction

This work is the result of a collaboration between myself Mr. Michele Pinelli, the University of California Irvine (UCI) Ph.D. candidate Hengje Wang, the University of California (UCI) Distinguished Professor Said Elghobashi and Professor Maurizio Quadrio of the Politecnico di Milano.
The main purpose of this thesis is to develop a code, based on finite differences, for the Direct Numerical Simulation (from now on DNS) of the incompressible Navier-Stokes equations to analyze the turbulent flow in an open channel with roughness on the bottom. The effect of the roughness on a turbulent flow is far from being understood. In fact there are a lot of difficulties researchers found, like how to model the roughness, how to define it, what solids to use and where to place them to model a real wall. The practical interests for these kind of research are a lot: from drag reduction for means of transport and oil pipes to the bacteria formation on the bottom of rivers. The application field is wide and that is why it is a very important topic. Unfortunately it is quite hard to simulate roughness and only very regular arrangement have been studied until now. In the last years a few attempts to study real roughness with DNS code has been made, one of the most important example being the study of Busse et al. [5], in which they used a surface scan as boundary condition for their flow. This is one of the most complicated case ever studied with a DNS until now, because usually the geometries used for this kind of simulations are very easy and the code cannot handle too complicated boundary conditions. This is a state of the art simulation and an exeption for DNS, we did not need such a performance and we decided to use spheres on the bottom of the channel in order to simulate roughness. One of the first attempt in this direction was made in 2011 by Chan-Braun et al. [8] and we chose it as the final validation of our code.
The request for this research came from the UCI Enviromental Engineering Departement, which was studying a Reynolds Averaged Navier-Stokes code to analyze the water flow over a river bed. In order to validate their method they asked to the UCI DNS team, supervised by Professor S. Elghobashi, to add an extention to the UCI DNS code, usally used for multiphase Homogenous Isotropic Turbulence (HIT from now on), in order to be able to handle an open channel flow with roughness. HIT and turbulent channel flow are quite different, because the former is usually considered the less complex case, there are no boundary conditions or forcing term[1], while in the channel flow there are two walls and also roughness in the case studied here. It should be kept

[1]It is not easy to define a forcing term for this case either, but usually the gravity acceleration is added to the Navier-Stokes equations and the fluid would flow in that direction without the need of a forcing term

in mind that HIT is an idealization never encountered in nature. A turbulent flow is said to be isotropic if rotation and buoyancy are not important (can be neglected) and there is no mean flow[2]. The presence of a mean flow with a particular orientation can introduce anisotropies in the turbulent velocity and pressure fields. It is already easy to see how different these two kinds of flow are, because in the channel flow the anisotropies are very important: they are the reason why the turbulence cycle exists, while the hypothesis of the HIT neglet their presence from the beginning. A flow is said to be homogeneous if there are no spatial gradient in any averaged quantity. This is equivalent to assume that the statistics of the turbulent flow is not a function of space; in the channel flow this hypothesis cannot be true, in fact the most important characteristics of this kind of turbulence is the fact that some gradient of pressure and velocity are there close to the wall. They are effects of the presence of the boundary condition and it is very important to consider the average of these fields in order to study the law of the wall for example. In a few words, HIT has hypothesis that, if applied, would not allow us to introduce any boundary condition in the flow, because they would create anisotropies or gradients of some field, that are what characterize the channel flow.
The channel flow code UCI DNS team developed until then was a $2D$ laminar channel flow. The main topic of this thesis is the development of this code and the comparison between the results we had at the different steps and the ones analyzed in papers published on important journals. The main purpose was to create a code able to perform the DNS of the case the Enviromental Engineering Departement was studying, being sure it would have given the correct results to validate their research. In order to do that we decided to start from the easiest case, the channel flow, and to add the more complex parts once we had the validation of the code we developed until then. We started from the $2D$ laminar channel flow code, computing the Poiseuille flow. Once we were sure the code was working we added the third dimension and the forcing term in order to be able to compare our code with Kim et al. [14]. After the first validation we imposed the free surface boundary condition on the top of the channel, to be closer to the final case of the river bed. In this case the validation was harder because of the lack of published papers on this topic; this is probably due to the fact that such an easy case is not interesting for research and usually, if present, it is used only for comparison. This was the case of the Chan-Braun et al. study [8], in which we had to digitize a graph in order to have the data for the comparison. In the end we added the last and most difficult part: the spheres on the bottom. The complexity of the computation and the code rose a lot, because we used the Immersed Bundary Method to define the surface of the particles. This was reflected on the results in which we found a small percentage of difference we did not find in the previous validations.
DNS is one of the most powerful tool to research on turbulent flow, but also one of the most expensive and problematic, because of the absence of turbulent model and the definition of boundary conditions respectively. This is the reason why this kind of simulation started to be studied in the seventies and the first reliable results were published in 1987 [14]. After this achievement the research kept going and it has not reached its limit even today. The increasing power of

[2]Rotation and buoyancy forces tend to suppress vertical motions and create an anisotropy between the vertical and the horizontal directions

processors has reached a limit few years ago and from then the number of cores used has been increased, becuase of the high demands of resources this kind of computation needs. Because of the same reason, in the last few years the researchers started to use GPU instead of CPU trying to overtake this development limit. Today the codes need to use powerful parallelisation algorithm in order to have the fastest possible computation time. The development of several DNS codes in history underlined the spectral method as one of the most efficient way to discretize the spatial domain for a channel flow. The solver from which the author started has been usually used for multiphase flows simulations; that is why UCI DNS team, supervised by Professor Said Elghobashi, developed a finite differences solver, considering it optimal for their kind of researches. In fact to handle the IBM code with a spectral code is quite complex and almost no one did that in the past. We decided then to keep as the same solver as the one developed in the past, because it would have been too time expensive to create a complete DNS code from the scratch. We kept also the same Immersed Boundary Conditions (from now on IBM) code, modifying it only in order to define the positions of the different spheres. Therefore the author developed the turbulent open channel flow from the scratch, using the already implemented solver and IBM routines.
The results we achieved are mainly statistics analysis of the code outputs defined in Chapter 2. The reason why we chose not to analyze other phenomenon, e.g. ejection or sweep, or develop the code to reproduce the case proposed by the Enviromental Engineering Departement till the end (considering also the movement of the contaminants in the rough wall) is that we found bigger differences in the last validation with the roughness: we considered useless to add more complex parts to a code unable to perform an easier case like the one studied by Chan-Braun et al. [8]. We focused our statistic analysis on the results of the publications, for each step we made we added different outputs to the program in order to compare it with the paper we were considering. At the end we had all the outputs shown in Chapter 2 and we were able to validate the code. These flow characteristics are important to understand the behaviour of the flow in the channel, because they allow us to observe the law of the wall and to compare every case with the others. It can be interesting to consider the differences on the mean velocity curve with and without spheres in order to understand the effect of the roughness on the turbulent flow e.g. how to add spheres on the bottom affect the turbulent flow statistics.
The structure of the thesis follows. In the first Chapter we defined the physical problem we accepted to simulate for the UCI Enviromental Engineering Departement, and it underlines the different aspects of the simulations and of the flow we wanted to analyze. This includes the description of the physical problem, the governing equations, a fast definitions of channel flow and open channel flow with their boundary conditions, the forcing terms used in the governing equations and a fast description of the complexity of the roughness. The second Chapter is a rapid excursus of the solver and the IBM code developed by the previous mentioned team, to make the reader understand how the code works and what kind of approximations were made. The third Chapter presents all the validations we made for the code, starting from the easiest ones and ending with the most important one. In this Chapter we show also the results of every validation and the values of the differences we found for our code. This is the main purpose of this thesis, because it was not possible to develop the full

problem described in the first Chapter due to the limited time we had. The last Chapter is the conclusion and the future possible development of this work.

The code developed is property of the University of California, Irvine and it will not be directly printed on this thesis.

# Chapter 1

# Flows over rough walls

The research on rough-wall turbulence focuses almost exclusively on the effect of the rough wall on the fluid. Some of the key questions of interest are how roughness influences the turbulence structure, what are the consequences for scaling, and how can the effect on the fluid be estimated from the roughness geometry. Most of the rough surfaces are irregular in nature, but researchers focused mostly on regular roughness geometry. This is due to the fact that we know such a few of this argument that we need to create basis before to be able to consider the real cases. The study of Schlichting [32], where roughness elements in the form of spheres, hemispherical caps and cones were arranged in uniform patterns, are a typical example. Other very common roughness configurations are surfaces composed by blocks and bars, because they are easy to build for wind tunnel experiments and they have an enough easy geometry to be represented in DNS codes. They are also easy to reproduce and they possess clearly defined ruoughness height. However, it is important to underline the fact that they cannot be used to define general roughness, because of their limited resemblance to irregular roughness. Highly regular rough surfaces can exhibit behaviour not commonly found for irregular rough surfaces. For example, a regular arrangement of roughness elements can lead to strong shielding (see [9]) or riblet effects (see [1]), in which there is an atypical reducion of drag due to the very regular position of cusps with all the same height. Therefore, the study of flow over irregular roughness cannot be replaced by studies of flow over highly regular rough surfaces, because these two kinds of surface have different effects on the flow. Moreover, roughness notably increases the complexity of turbulent flows, for this reason, despite their great relevance, little is known about it, even in simple geometries.
In this Chapter, a brief state of the art for turbulent flows over rough walls is proposed.

## 1.1 Physical problem

The turbulent transport of mass to a stream-bed is integral to many global bio-geochemical cycles, and plays a key role in the mobility and toxicity of anthropogenic contaminants and their impact on human and ecosystem health. For example, nutrient uptake by algae growing on the bottom of a stream is

variously controlled by stream hydrodynamics or cell uptake, depending on the strength of turbulent mixing near the bed. When near-bed turbulent mixing is low (e.g., at lower stream velocities) nutrient transfer is rate-limited by the downward mixing of nutrient–rich waters (mass-transfer limited conditions). On the other hand, when near-bed turbulent mixing is high (e.g., at higher stream velocities) nutrient uptake is rate-limited by the rate at which algal cells can take up nutrients across their cell walls (uptake-limited conditions). There are many such examples where the transport and transformation of aquatic contaminants depends on a delicate balance between near-bed turbulent mixing and biological processes.
Bed roughness increases mass transfer to the sediment bed by several mechanisms. Generally speaking, hydrodynamically rough beds are also highly permeable; e.g., in non-cohesive sediments the Kozeny-Carmen equation predicts that sediment permeability increases with the square of the median grain diameter in a laminar flow (see Appendix A.1). This combination of roughness and permeability enhances mass transfer across the sediment-water interface by a number of interrelated mechanisms, including:

- sweep and eject events become more intense, particularly on the downstream side of individual roughness elements (e.g., cobbles) where boundary layer separation can occur

- sweep and eject events penetrate some distance into the sediment bed carrying with them both mass and fluid momentum

- sweep and eject events generate long-period pressure waves that pump water into and out of the sediment bed as the waves travel horizontally through the water columns

For all of these reasons, measured mass transfer coefficients increase sharply with increasing sediment bed roughness, in some cases by a factor of 10 or more. This is the reason why a lot of studies on turbulent flows over rough walls have been performed for thirty years.

## 1.2 Law of the wall

Before to start describing the roughness effect on a turbulent flow it is important to describe the behaviour this kind of flow have in the smooth case. In order to do that we have to introduce some important definitions. All of them are peculiar of the channel geometry and they are fundamental to define the turbulent flow developed with those boundaries (for an appropriate description of the channel flow geometry and boundary condition see Chapter 2). The first variables that must be introduced are the mean velocities $U, V$ and $W$ and their fluctuations $u, v$ and $w$. If we consider $H$ as half of the vertical height of the channel we can define the bulk velocity:

$$U_b = \frac{1}{H} \int_0^H \langle u \rangle \, dy \tag{1.1}$$

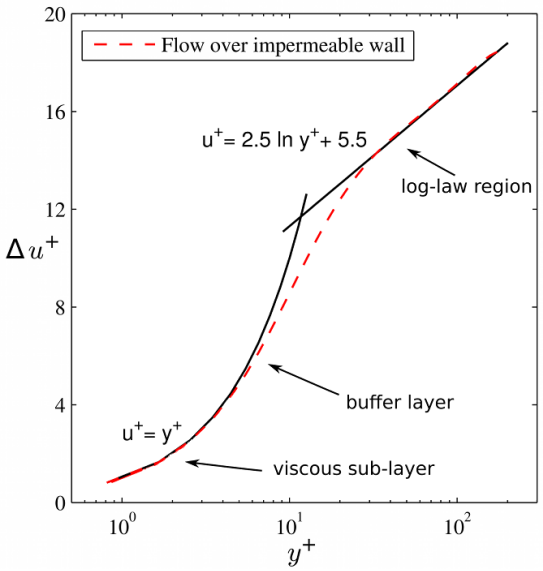


Figure 1.1: Theoretical law of the wall in viscous and logarithmic region

Other important variables are:

$$\tau = \rho\nu \frac{d\langle u\rangle}{dy} - \rho\langle u'v'\rangle \tag{1.2}$$

$$\tau_w = \tau(0) = \rho\nu \left.\frac{d\langle u\rangle}{dy}\right|_0 \tag{1.3}$$

$$u_\tau = \sqrt{\frac{\tau_w}{\rho}} \tag{1.4}$$

$$\delta_\nu = \nu\sqrt{\frac{\rho}{\tau_w}} = \frac{\nu}{u_\tau} \tag{1.5}$$

where $\tau$ is the shear stress, $\rho$ the density of the fluid, $\nu$ the kinematic viscosity, $\tau_w$ is the shear stress at the wall, $u_\tau$ is the friction velocity and $\delta_\nu$ is the viscous lengthscale. These quantities are useful to define the flow through the friction Reynolds number:

$$Re_\tau = \frac{u_\tau H}{\nu} = \frac{H}{\delta_\nu} \tag{1.6}$$

Once the flow is statistically stable different regions can be defined. All of them can be located using the viscous length:

$$y^+ := \frac{y}{\delta_\nu} = \frac{u_\tau y}{\nu} \tag{1.7}$$

As underlined in Pope's book [29], "$y^+$ is similar to a local Reynolds number, so its magnitude can be expected to determine the relative importance of viscous and turbulent processes. [...] In the viscous wall region ($y^+ < 50$) there is a direct effect of molecular viscosity on the shear stress, while in the outer layer ($y^+ > 50$) the effect of viscosity are negligible. In the viscous sublayer ($y^+ < 5$)

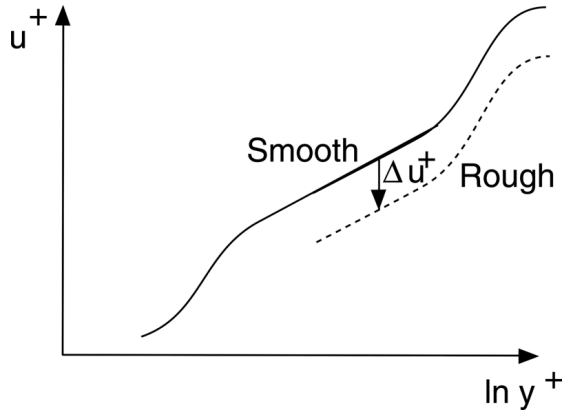


Figure 1.2: Definition of $\Delta u^+$ in order to describe the difference between a flow over a rough and a smooth wall in the law of the wall

the Reynolds shear stress is negligible compared to the viscous term. As the viscous Reynolds increases the fraction of the channel occupied by the viscous wall region decreases."
Different studies on this behaviour allowed the researchers to define a mathematical law to describe this phenomenon. The flow close to the wall can be modelled quite well by:

$$u^+ = y^+ \tag{1.8}$$

As can be seen in Figure 1.1 the model is quite good until $y^+ < 5$, where the viscous effects are prevalent. On the opposite, for larger $y^+$, the curve can be well described by the log law:

$$u^+ = \frac{1}{\kappa} ln(y^+) + B \tag{1.9}$$

where $\kappa$ is the Kolmogorov constant and it is usually close to 0.41 and B is a constant usually close to 5.2 (with a 10% of difference in the vaiours studies). Between these two regions there is the buffer layer which is not described by any mathematical model. All of these regions together define the inner layer which extends until $y^+ = 1000$. In this thesis the flow has been considered bounded by two vartical walls that limits the extension and consequentely a channel flow does not have an outer layer, that is why the theory about it will not be described here.

## 1.3 Roughness

First of all it is important to define how roughness has been modelled until now. In history different types of roughness has been encountered in engineering and environmental flows that make it worthwhile trying to establish a meaningful classification for this phenomenon. In order to do that a roughness function, or shift of the mean velocity profile relative to a smooth wall $\Delta u^+$ (as can be seen in Figure 1.2), has been defined. This function depends on the density, height, and nature of the roughness. Two different type of roughness became commonly

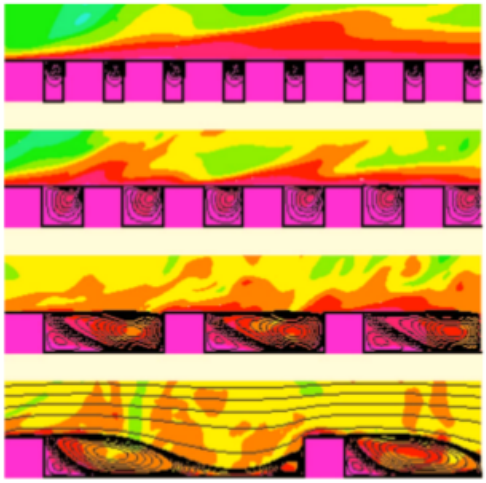

Figure 1.3: Instantaneous passive scalar contours superimposed on mean streamlines. From top to bottom, $\frac{w}{k} = 0.5, 1, 3, 7$. From Leonardi et al. [19] study.

accepted in history: "k-" and "d-" type behaviour.
We have a k-type roughness when, having a rough surface made up of transverse square bars, the cavity width $w$ is larger than the height $k$; $\Delta u^+$ is then a function of the roughness height as follows:

$$\Delta u^+ = \frac{1}{\kappa} ln(k^+) + C \tag{1.10}$$

where $\kappa$ is a universal constant and $C$ depends on the nature and density of the roughness. Bisceglia et al. [3] found that, for two-dimensional square bars, the roughness function follows Equation 1.10, but with $\kappa = 0.61$. For the same surface, Perry et al. [28] did not find any correlation between $\Delta u^+$ and $k^+$ and proposed that for this type of roughness, referred to as d-type, $\Delta u^+$ should be given by

$$\Delta u^+ = \frac{1}{\kappa} ln(d^+) + D \tag{1.11}$$

where $D$ depends on the nature and density of the roughness. These authors suggested that for a k-type roughness, eddies with length scale of order $k$ are shed into the flow above the crests of the elements, diffusing into the flow. On the other hand they considered the d-type roughness elements too closely spaced to create this phenomenon, impling that the dfference between the two types of roughness is mainly the eddy shedding from the surface to the flow. On the contrary, other studies, like Djenidi et al [11] and Leonardi et al. [18], found that vortex shedding out of the cavities is present also for $w/k = 1$, proving that this definition cannot be universal. The value of $w/k$ defines the intensity of the ejections: there are very strong ejections for values between 3 and 9, but the transition from $w/k = 1$ to 3 and 9 appears to be rather gradual. Therefore, the abrupt transition between d-type and k-type behavior cannot simply be explained by the vortex shedding out of the cavities. Orlandi et al. [26] found that

the roughness function for both d- and k-type roughness, collapsed into a single curve when plotted as a function of the rms wall-normal velocity at the crests plane. Since the rms velocity is correlated with the shedding out of the cavities, the nature and intensity of the shedding cannot explain the abrupt transition between d- and k-type roughness.
The distinction between the two types of roughness remains unclear. Some studies suggested $w/k = 3$ as the demarcation line between k- and d-type behaviour, but others considered this value as k-type roughness. This is probably due to the fact that accurate mesurements near the wall are not possible, in particular the values of wall shear stress and the position of the origin are unknown. In fact, every author defines his own parameters, making the comparison bewteen different studies full of uncertainties. Several ways to estimate the origin position in a DNS code are described in the Appendix ofChan-Braun et al. [14]. In this paper the authors estimate the wall shear stress extrapolating the data from the vaues over the spheres with a linear function. DNS, albeit at lower Reynolds numbers, provide reliable values of $U_\tau$ and error in origin.
The most important study about the difference between k- and d-type roughness was made by Leonardi et al. [19] in which a new definition for k- and d-type behaviour was introduced, thanks to DNS studies with different Reynolds Numbers and $w/k$ values. The most important results of this study was that for d-type roughness the roughness function does not depend on $k^+$ and that the difference between k- and d-type roughness is related to the relative magnitudes of the frictional and pressure drags.

## 1.4 Experimental researches

A number of experimental studies have investigated flow over regular and irregular roughness; a reference for the earlier work on roughness is Schlichting [32], but the best known example is considered the study of Nikuradse [23] on turbulent flow over rough surfaces made from sieved sand grains. This approach was adopted by others, e.g. rough surfaces made up from sand and round pebbles have been used in flow channel experiments (see [13]), while packed gravel chips (see [7]), abrasive sheets (see [27], [2]]) and scratched surfaces (see [33]) have been used to produce rough surfaces for wind tunnel experiments. In most cases, these surfaces have been used as a convenient way to construct a rough surface with a reasonably well defined roughness height and not necessarily because they were of particular practical interest. A good example would be the study of Nikuradse cited before, which tried to define a general constant $k$ to compare different roughness surfaces. Unfortunately this constant is connected to regular sand-roughness and cannot be used for every type of it. This make us understand how wide this field could be: researchers should study every material on the Earth and define a constant for each of their surfaces, that it seems quite unpractical. With the advent of better moulding techniques and 3D printing, rough surfaces models, which are based on roughness found in technical applications, have started to be used in rough-wall turbulent flow experiments. Bons [4] used scaled models of rough surfaces based on scans of damaged turbine surfaces in wind tunnel experiments. A systematic study of the effect of irregular roughness on turbulent channel flow using roughened steel plates was conducted by Rij et al. [36]. Some aspects of rough-wall flows at high Reynolds

number have been reviewed by Marusic et al. [21], in particular the question of whether roughness does indeed modify the turbulence structure in the outer flow or simply provides a modified friction velocity. It is easy to see that we are quite far from understanding this phenomenon and its effects on the flow also in wind tunnels, where the actual rough surface studied can be used.

## 1.5 Numerical researches

DNS is the computer killing application and the more complicated the geometry the more expensive are the computation; numerical studies of rough-wall flows are very demanding in terms of computational cost, much more so than comparable simulations of flow over smooth walls. Therefore, fewer DNS studies of flow over rough walls have been carried out so far than of flows over smooth walls. With this concept in mind, we can analyze the different works in which researchers tried to simulate a very complex phenomenon like the surface roughness.
As stated before, it is hard to make effective wind tunnel experiment on roughness because of its nature; it is quite obvious then that to model it in a computer code is much harder and in a DNS, able to handle only simple geometry, can be almost impossible. This is the reason why a few DNS studies on regular roughness have been performed in the last thirty years, but almost none on the irregular case. Examples of studies on regular roughness are Lee and Sung [15] and Lee et al. [16], in which they used rectangular spanwise bars and cubes, Leonardi et al. ([19] [17]) among others considered a wall similarly roughened by spanwise-oriented square bars, while Orlandi and Leonardi [24] have simulated plane channel flow including different layouts of wall-mounted cubes. In the studies of Orlandi et al. [25] and Flores and Jiménez [12] a DNS of channel flow with wall velocity disturbances, put there in order to simulate an artificial roughness, have been carried out. Closer to the present thesis Singh et al. [34] performed a DNS of a channel flow over an hexagonal arrangement of spheres, with a much coarser resolution than the one considered in the Chan-Braun et al. [8] study. In the latter paper a regular roughness was modelled thanks to 9216 spheres placed on the bottom wall of an open channel and the study focused on the forces acting on the spheres and the erosion effects due to this phenomenon.
Only a small number of highly resolved numerical studies have been performed on turbulent flow over irregular roughness. Napoli et al. [22] studied flow over irregular wavy rough surfaces. In these simulations the roughness was uniform in the spanwise direction. In a recent study, Cardillo et al. [6] investigated the development of a turbulent boundary layer over a surface that was based on a laser scan of sandpaper. The most important study in this direction was done by Busse et al. [5], in which they used the scan of a graphite surface in order to simulate irregular roughness. All of these studies are the current state of the art of DNS of irregular roughness surfaces.

## 1.6 Present work

The present work is aimed to validate our code with the study of Chan-Braun et al. [8]. Consequentely we are going to consider an open channel flow with a regular arranged roughness on the bottom surface modelled by 9216 fixed spheres. This is a first step to develop a future code able to consider the movements of the contaminants inside this kind of roughness. This thesis focuses only on the validation of the code developed until now: we are going to compare the statistics of the turbulent flows over the same rough bottom with a coarser grid size and the same grid size of the paper written by Chan-Braun et al. [8]. After this a comparison between the behaviour of a turbulent channel flow over a rough and a smooth surface will be made in order to understand if our code can give us the correct results; in fact, using a different forcing term strategy did not allow us to have a perfect match of the results, we had to see if the behaviour found by our code was correct compared to the theoretical law of the wall. Of course this is not a sure validation because this theory is far from being considered universal (as previously understand), but it gave us the idea that we are in the right direction with the development of the DNS code.

# Chapter 2

# Description of the method

In the following Chapter we are going to present the hypothesis we had to impose in order to be able to represent the physical problem previously described with a DNS; to do so we had to define the boundary conditions and to model the roughness on the bottom surface. In the following, all of the approximations and a small description of the numerical method developed to achieve this purpose are presented.

## 2.1 Channel flow

We consider now the configuration shown in Figure 2.1. We have a length $L$ and a width $b$, with walls to restrain the vertical domain with a distance of $2H$ between each other. We consider the channel indefinetely long ($L/H >> 1$) and wide ($b/H >> 1$); this kind of configuration is called plane channel flow.
The chosen reference system is shown in Figure reffig:channel and it is composed by the following directions:

- $x$: it has the mean flow direction: streamwise direction
- $y$: it is perpendicular to the walls and to the $x$-axis: crossflow direction
- $z$: it is parallel to the walls and perpendicular to the $x$-axis: spanwise direction

$x$- and $y$-axes are usually called homogenous directions of the flow. The position of the walls on the $y$-axis will be then $y = \pm H$. The Reynolds number is usually computed considering half of the channel height $H$.

### 2.1.1 Boundary conditions

The boundary conditions considered in this problem are the one used inKim et al. [14]. The walls have no-slip and no-penetration boundary conditions: $u = 0$. We have that the velocity at the wall is zero due to the boundary layer constraint.
The use of periodic boundary conditions in the $x$- and $z$-direction allows us to consider the channel as indefinitely wide in those directions. This means that, in reality, we are considering the flow far away from any solid bounday, e.g. walls,

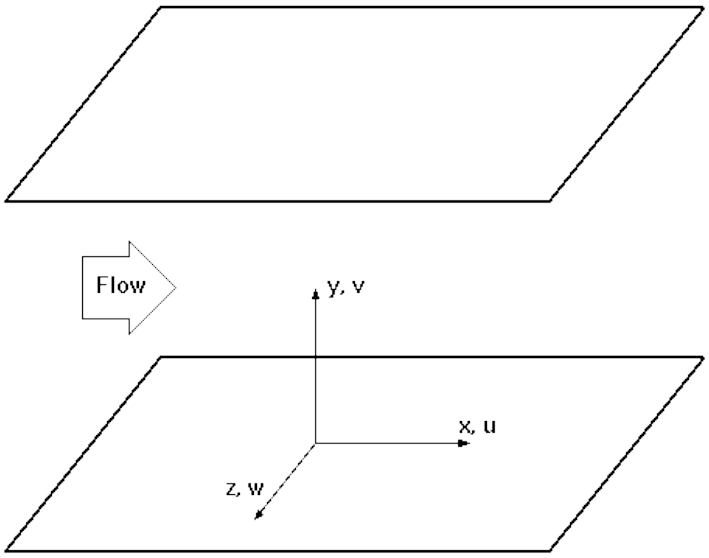


Figure 2.1: Sketch of the channel flow

river banks, inlet or outlet of the river. In this way it was possible to consider a completely developed flow and study its statistics as monodimensional; in fact the crossflow direction is the only one in which the statistics can change, because of the boundary conditions on the walls. It is easy to see that in the real case $x$- and $z$-directions have physical boundaries, periodic boundary conditions are only an artifice to consider the channel indefinetely wide.

## 2.2 Open channel flow

We are now considering only half of the channel described above and we add a rough bottom. This configuration is shown in Figure **??**. It is easy to notice that nothing has changed in the reference system respect to previous case.
The geometry shows that we have, as before, an indefinite domain in the homogenous directions $x$ and $z$, an open surface at $y = H$ and the wall at $y = 0$. All the considerations made before to the length and the width of the channel can be applied also in this case. We have now only half of the height we had before, our vertical distance between the wall and the free surface will be $H$. It is important to notice that, this time, the Reynolds number is computed considering the total height $H$ instead of half of it, because we are considering only half of the channel.

### 2.2.1 Boundary conditions

The boundary conditions considered in this problem are the one used inChan-Braun et al. [14]. The top wall has a null Neumann boundary condition, we have then that $\partial u/\partial y = 0$. This is due to the fact that, at the free surface of the river, the flux is free to flow at the velocity imposed by the shear stress of the streamline below and it has no restraints from the top. It is easy to see that

the shear stress on the top surface is null and then we have a zero derivative of the velocity.
The bottom wall has no-slip and no-penetration boundary conditions, because of the presence of the wall. We have that the velocity at the wall is zero due to the boundary layer constraint. The boundary conditions on the spheres are described in the following Chapter.
The use of periodic boundary conditions in the $x$- and $z$-direction allows us to consider the channel as indefinitely wide in those directions. This means that, in reality, we are considering the flow far away from any solid bounday, e.g. walls, river banks, inlet or outlet of the river. In this way it was possible to consider a completely developed flow and study its statistics as monodimensional, because the crossflow direction is the only one in which it can change because of the boundary conditions on the top and on the bottom. It is easy to see that in the real case $x$- and $z$-directions have not physical boundaries, periodic boundary conditions are only an artifice to consider the the channel indefinetely wide.

## 2.3 Governing equations

The governing equations for an incompressible turbulent flow are the Navier Stokes equations

$$\frac{\partial u_i}{\partial t} + \frac{\partial (u_i u_j)}{\partial x_j} = -\frac{1}{\rho}\frac{\partial p}{\partial x_i} + \nu \frac{\partial^2 u_i}{\partial x_j \partial x_i} + F_i \tag{2.1}$$

and the continuity equation

$$\frac{\partial u_i}{\partial x_i} = 0 \tag{2.2}$$

where $i = 1, 2, 3$ are the three coordinate directions $x$, $y$, $z$, $p$ the pressure, $\rho$ the density, $\nu$ the kinematic viscosity of the fluid, $f_i$ the forcing term and $u_i$ the velocity in the $x_i$ direction, respectively.
Note that (2.2) and (2.1) are written in non-dimensional form, and throughout the thesis all variables are dimensionless except those with superscript $\bar{\cdot}$.

### 2.3.1 Forcing term

The only component of the forcing term $F_i$ is $F_1$ (in the x-direction), because $F_2$ is zero, due to the fact that no flow rate or pressure difference can exist between the two impermeable walls and very often it is also considered that $F_3 = 0$.
There are three different strategies to define the forcing term in the Navier-Stokes equations (2.1) described by Quadrio et al. [30]:

- Constant Pressure Gradient (CPG)
- Constant Flow Rate (CFR)
- Constant Power Input (CPI)

Two ways to define the forcing term were developed in our code: CPG and CFR. CPG has been used in every case analyzed, while CFR, although developed for both the smooth and the rough case, has been used only in the smooth case.

**Constant Pressure Gradient**

The easiest way to define the forcing term is CPG, because we needed only to replace it with a constant pressure gradient:

$$F = -\left\langle \frac{dp}{dx} \right\rangle \tag{2.3}$$

The pressure gradient value was defined considering that it had to balance the shear stress at the wall $\tau_w$:

$$\left\langle \frac{dp}{dx} \right\rangle = -1 \tag{2.4}$$

In this case it is simple to demonstrate that, being the velocity non-dimensionalized with the friction velocity $u_\tau$, the Reynolds number is:

$$Re_\tau = \frac{u_\tau \delta}{\nu} \tag{2.5}$$

In this case $Re_\tau$ is imposed and we need to find $U_b$ and $Re_b$. Our code gave us the mean velocity data in every center of the grid point, so it was easy to find $U_b$ from its definition:

$$U_b = \frac{1}{H} \int_0^y \langle u \rangle \, dy \tag{2.6}$$

where $\langle u \rangle$ is the mean velocity averaged on $x$, $z$ and the time. To find $Re_b$ we can define:

$$\frac{Re_b}{Re_\tau} = \frac{U_b}{u_\tau} \tag{2.7}$$

We can write:

$$\frac{U_b}{u_\tau} = \frac{\overline{U_b}}{\overline{u_\tau}} = \frac{\overline{U}_b}{\overline{u}_\tau} \tag{2.8}$$

but in this case (CPG) the bulk velocity is already non-dimensionalized with $u_\tau$:

$$\frac{\overline{U}_b}{\overline{u}_\tau} = U_b \tag{2.9}$$

Then we can easily find:

$$Re_b = Re_\tau \frac{U_b}{u_\tau} = Re_\tau U_b \tag{2.10}$$

**Constant Flow Rate**

This case is more complicated than the previous one, because the forcing term changes at every time step. The advantage is that it allows to have a faster transient. The method can be summerized as follows:

1. It splits the velocity field in two components:

$$u_1^{n+1} = \tilde{u}_1^{n+1} + \hat{u}_1^{n+1} \tag{2.11}$$

   Where $\hat{u}_1^{n+1}$ is the solution of the Navier-Stokes equations imposing a null forcing term ($F^{n+1} = 0$), while $\tilde{u}_1^{n+1}$ is the corrective solution we impose to have the constant flow rate condition satisfied.

2. Replacing the splitted velocity in the first component of the discretized Navier-Stokes equations:

$$\tilde{u}_1^{n+1} = \Delta t \left( F^{n+1} + \frac{1}{2\,Re} \frac{d^2 \tilde{u}_1^{n+1}}{dy^2} \right) \tag{2.12}$$

Imposing the boundary conditions it is possible to find the solution:

$$\tilde{u}_1^{n+1} = \Delta t F^{n+1} [1 - e^{-\lambda t}] \quad \wedge \quad \lambda = \sqrt{\frac{2Re}{\Delta t}} \tag{2.13}$$

From the definition of bulk velocity the forcing term can be computed:

$$\Delta u_b^{n+1} = \int_0^H \tilde{u}_1^{n+1} dy = \Delta t F^{n+1} \left( 1 - \sqrt{\frac{\Delta t}{2\,Re}} \right) \tag{2.14}$$

Where $\Delta u_b^{n+1}$ is defined by $\hat{U}_b^{n+1}$ and imposing:

$$\tilde{U}_b^{n+1} = 1 \tag{2.15}$$

Getting in the end:

$$\Delta u_b^{n+1} = \tilde{U}_b - \hat{U}_b^{n+1} \tag{2.16}$$

Now we can see that the only unknown in Equation 2.14 is $F^{n+1}$

3. Now it is possible to find the corrective velocity field imposing the forcing term found in the previous step:

$$\tilde{u}_1^{n+1} = \Delta t F^{n+1} [1 - e^{-\lambda t}] \tag{2.17}$$

4. In the end the velocity field can be found throughout Equation 2.11

In the case with the spheres this method is much more complicated, because the area of the channel in every slice is different and it is necessary to impose a different $U_b$ for all of them. With the code developed an error of 0.4% on the flow rate was found: it was considered inadmissible being the code based on this value.
In this case the Reynolds number wll be based on $U_b$, being the velocity non-dimensionalized through the bulk velocity. In is necessary to find the non-dimensional variables based on the friction velocity, because the output velocity was non-dimensionalized by $U_b$. The output velocity reads:

$$u = \frac{\overline{u}}{\overline{U}_b} \tag{2.18}$$

For the comparison is common to use the viscous velocity:

$$u^+ = \frac{\overline{u}}{\overline{u}_\tau} \tag{2.19}$$

It was needed to "convert" the output velocity to the comparable one[1]:

$$u^+ = \frac{\overline{u}}{\overline{u}_\tau} = \frac{\overline{u}}{\overline{U}_b} \frac{U_b}{u_\tau} \tag{2.20}$$

[1] we considered Equation 2.8

Considering the definition of $u_\tau$:

$$\frac{u_\tau}{U_b} = \frac{\sqrt{\nu \frac{d\tilde{u}}{d\tilde{y}} \frac{U_b}{H}}}{U_b} = \frac{U_b \sqrt{\frac{d\tilde{u}}{d\tilde{y}} \frac{\nu}{U_b H}}}{U_b} = \sqrt{\frac{d\tilde{u}}{d\tilde{y}} \frac{1}{Re_b}} = \sqrt{\tau_w} \tag{2.21}$$

Consequently:

$$u^+ = \frac{u}{\sqrt{\tau_w}} \tag{2.22}$$

$Re_\tau$ can be easily find having the ratio between the friction and the bulk velocities:

$$Re_\tau = Re_b \frac{u_\tau}{U_b} = Re_b \sqrt{\tau_w} \tag{2.23}$$

## 2.4 Numerical method

The UCI's DNS method solves the unsteady three-dimensional Navier–Stokes equations (2.1) and continuity equations (2.2) throughout the whole computational domain $\mathcal{D}$, including the interior of the dispersed particles. These governing equations are discretized in space in an Eularian framework using a second-order finite-difference scheme on a uniform staggered mesh. Time integration was performed via the Adams–Bashforth second-order scheme with a time step $\Delta t = \frac{\Delta x}{2}$, where $\Delta x$ is the grid spacing. Pressure was treated implicitly and was obtained by solving the Poisson equation in finite-difference form using a combination of a two-dimensional fast Fourier transform (FFT) in the $x_1 x_2$ plane, and Gauss elimination in the $x_3$ direction.

### 2.4.1 Immersed Boundary Method

The fluid acceleration due to the inertia and viscous forces reads:

$$RU_i = -\frac{\partial (u_i u_j)}{\partial x_j} + \nu \frac{\partial u_i}{\partial x_j \partial x_j} \tag{2.24}$$

Equations (2.1) can be re-written in a compact form as:

$$\frac{\partial u_i}{\partial t} += -\frac{1}{\rho} \frac{\partial p}{\partial x_i} + RU_i + f_i \tag{2.25}$$

where $p'$ is the pressure non-dimensionalized with the kinematic viscosity and the density.
The flow solver has the following five steps:

1. the time integration of (2.1) without the pressure and forcing terms is performed through the Adams-Bashforth scheme:

$$\frac{u_i^* - u_i^n}{\Delta t} = \frac{3}{2} RU_i^n - \frac{1}{2} RU_i^{n-1} \tag{2.26}$$

where $u_i^*$ is an approssimation of $u_i^{n+1}$ before applying the forcing and the pressure corrections.

2. The instantanous force components $f_i$ are computed as follows:

$$U_i\big(\boldsymbol{X}_l^{(m)}\big) = \sum_{x\in\mathcal{D}} u_i^*(\boldsymbol{x})\,\delta_h\big(\boldsymbol{x}-\boldsymbol{X}_l^{(m)}\big)h^3 \qquad \forall\, l,m \tag{2.27}$$

$$F_i(\boldsymbol{X}_l^{(m)}) = \frac{U_i^{(d)}(\boldsymbol{X}_l^{(m)}) - U_i^*(\boldsymbol{X}_l^{(m)})}{\Delta t} \qquad \forall\, l,m \tag{2.28}$$

$$f_i(\boldsymbol{x}) = \sum_{n=1}^{N_p}\sum_{l=1}^{N_l} F_i(\boldsymbol{X}_l^{(m)})\,\delta_h\big(\boldsymbol{x}-\boldsymbol{X}_l^{(m)}\big)\,\Delta V_l^{(m)} \tag{2.29}$$

   where the lower-case letters denote quantities computed at the Eulerian mesh points $\boldsymbol{x}$, and the upper-case letters denote quantities computed at the Lagrangian force points $\boldsymbol{X}_l^{(m)}$, with $1 \le m \le N_p$ and $1 \le l \le N_l$, where $N_p$ is the number of particles tracked and $N_l$ is the number of Lagrangian force points distributed uniformly over the surface of each particle.

3. The force imparted by the particle is applied by updating $u_i^*$:

$$\hat{u}_i^* = u_i^* + \Delta t f_i \tag{2.30}$$

4. The pressure is computed by solving the Poisson equation:

$$\nabla^2 p^{n+\frac{1}{2}} = \frac{\frac{\partial \hat{u}_j^*}{\partial x_j}}{\Delta t} \tag{2.31}$$

5. The fluid velocity is corrected with the pressure gradient according to:

$$u_i^{n+1} = \hat{u}_i^* - \Delta t\,\frac{\partial p^{n+\frac{1}{2}}}{\partial x_i} \tag{2.32}$$

The projection method ((2.26) (2.30) (2.31) (2.32)) is second-order accurate in space and time for the velocity $u_i$, but first-order accurate in time for the pressure, $p$. Since the computed pressure is used exclusively to impose the condition of divergence-free velocity, the presented results are not affected by the lower-order pressure. [20]

# Chapter 3

# Validation for the smooth channel flows

In the following sections all of the validations made for a smooth channel flow are presented. As first validation we implemented the code to reproduce the results of the Kim et al. [14] paper and then we modified the geometry to become as the same as in the Chan-Braun et al. [8] study. The flow was considered statistically stable once the total shear stress (Equation A.3) was linear. We are going to show the validations we had with the code described above.
All of the outputs of our program gave us the possibility to analyze different aspects of the flow; of course we chose to display the results given in the papers so we could compare our code with theirs. We decided to show the shear stresses to demonstrate that the code was statistically stable and the average appropriate, the mean velcity profile (interpolated from the the DNS data) to have a fast and direct way to see if the results given by our code were correct before the next computation and, for the sphere case, we considered the three averaged components of the Reynolds stresses. In the end we computed the friction coefficient $C_f$ in order to define the reliability of our computations: we define this quantity in the following sections because its definition is different in the different cases.

## 3.1 Channel flow

We chose to use the Kim et al. [14] study as first comparison, because it is one of the most duplicated DNS work in history and, because of that, one of the most reliable.
In the paper the authors used a domain size of $4\pi H \,\mathrm{x}\, 2H \,\mathrm{x}\, 2\pi H$, we define here $H$ as half of the dimensonal vertical dimension of the channel. Being our code based on finite differences, instead of spectral method, we decided to approximate this domain in the following manner: $12H \,\mathrm{x}\, 2H \,\mathrm{x}\, 6H$, avoiding to use the periodicity introduced by $\pi$. It is possible to see the geometry in Figure 2.1.
The input of our program is $Re_\tau$ from which we can define every quantity; in this case $Re_\tau$ is 180. The average on the first velocity component was made, as defined in the paper, in the $x$ and $z$ direction and in time. We used different

grid-size in order to study the scalability of our code:

**Coarser grid-size** The grid-size we used is slightly different from the one in the paper, because our code has always worked with a uniform grid. We decided not to change this characteristic because in the following validation with the Chan-Braun et al. [8] paper we will use a uniform grid-size. We decided to keep the value in the $y$-direction, being it the most important, and to scale all the other values consequently, so our grid-size was $768 \times 128 \times 384$ instead of the $192 \times 129 \times 160$ used in the paper. The use of a uniform grid-size did not allow us to reach the same positions close to the wall that the authors got in the paper with an adaptive method of course; anyway we considered the fact that they used maybe too much points close to the wall for the results reached.
After the flow was completely develped we chose to make the mean over 20 time units, because we noticed that increasing the observation time did not give us different results.

**Finer grid-size** After the previous validation the grid points were doubled in every direction. This simulation was made in order to introduce in the code the possibility to use the results from a previous computation, with half of the grid points in every direction, as initial conditions for a finer grid-size. This result was achieved using a three dimensional interpolation of the points. The only variable different from the previous computation is the grid-size, which in this case was $1536 \times 256 \times 768$.

### 3.1.1 Comparison

We compare now our channel flow code with the results of Kim et al. [14]. The results of the grid-size of Kim et al. [14] (coarser grid-size) and a finer grid-size are following.

**Coarser grid-size** It is possible to notice in Figure 3.1 that the flow is statistically stable and that all the components of the total shear stress are correct. We defined here:

$$\tau_t = \tau_{Re} + \tau_{visc} = -\langle uv \rangle + \frac{1}{Re} \frac{d\langle u \rangle}{dy} \tag{3.1}$$

where $\tau_t$ is the total shear stress, $\tau_{Re}$ is the Reynolds shear stress and $\tau_{visc}$ is the viscous shear stress. We decided to compare the results of the the mean velocity in normal and logarithmic axis, as shown in Figure 3.2 and Figure 3.3, respectevely. This last Figure is useful to detect easily the difference in the two curves. It is clear from the shapes close to the wall that our grid points in that position are much less compared to the ones of the paper, as previously written. This difference is important because the production of turbulence starts close to the wall; it is quite easy to connect this fact to the difference in the center-line velocity. Anyway the differences we found in the mean velocity are very small and we considered the validation completely satisfactory.

| | Kim et al. [14] | our code |
|---|---|---|
| $C_{f0}$ | $6.00 \cdot 10^{-3}$ | $6.00 \cdot 10^{-3}$ |
| $C_f$ | $8.14 \cdot 10^{-3}$ | $8.18 \cdot 10^{-3}$ |

Table 3.1: Comparison between the friction coefficients found by our code e by Kim et al. [14] for the coarser grid-size case

| | Kim et al. [14] | our code |
|---|---|---|
| $C_{f0}$ | $6.00 \cdot 10^{-3}$ | $6.04 \cdot 10^{-3}$ |
| $C_f$ | $8.14 \cdot 10^{-3}$ | $8.21 \cdot 10^{-3}$ |

Table 3.2: Comparison between the friction coefficients found by our code e by Kim et al. [14] for the finer grid-size case

We computed the friction coefficients as described in Kim et al. [14]:

$$C_f = \frac{\tau_w}{\frac{1}{2}\rho U_b^2} \tag{3.2}$$

$$C_{f0} = \frac{\tau_w}{\frac{1}{2}\rho U_c^2} \tag{3.3}$$

where $U_c$ is the velocity in the center-line. The values we found are compared with the Kim et al. [14] ones in Table 3.1. The difference in the second definition of the friction coefficient is probably due to the fact that we used a uniform grid-size and, being this characteristic very important for the development of the flow, our turbulence was slightly "different" from the one found in the paper (e.g. we lose some phenomenon close to the wall). Anyway we can consider a difference of 0.5% completely admissible and the validation acceptable.

**Finer grid-size** The flow is statistically stable as shown in Figure 3.4. From this Figure we can see that the behaviour at the wall is better represented, because of the bigger number of points at the wall. Anyway this number is much smaller than the case developed in the paper because of the uniform grid-size restraint.
As previously done we computed the friction coefficients getting with the results in Table 3.2: It is possible to notice that the results are worse than the previous case; this can be explained by the fact that doubling the points in every direction means to use eight times the grid-size and to be able to capture phenomena eight times smaller than in the previous case. Because of that we can consider the flow evolving in a different way and to develop a "slightly different" turbulence. This is underlined by the behaviour of the mean veocity, shown in Figure 3.5 and Figure 3.6. It is clear how our code underestimates the velocity in the center-line, but the slope is closer in the "logarithmic" region. Looking at the values found for the friction coeeficients it is easy to see that these differences are very small and they cannot be considered to be relevant: the values found are

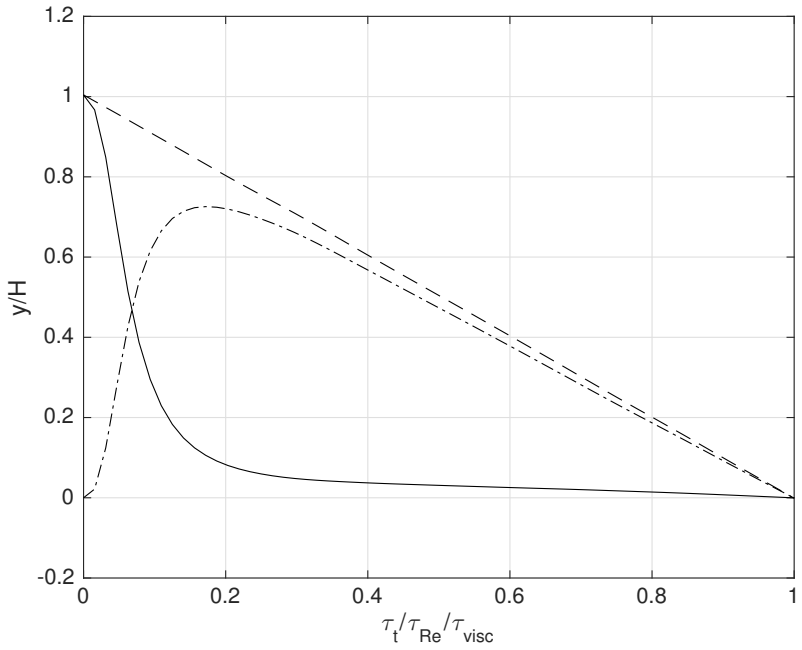


Figure 3.1: Shear stresses non-dimensionalized by $Re_\tau$ with the y grid-size of Kim et al. [14] for channel flow

satisfactory and we can consider the validation valid. Of course it is clear from Figure 3.6 that the points close to the wall are again much less than in the case studied in the paper.

## 3.2 Open channel flow

After the first validation we imposed the Neumann boundary condition on the top of the channel, to be closer to the rough case analyzed later. In this case we changed also the dimensions of the channel, using the ones defined in Chan-Braun et al. [8] study: $12H \times 1H \times 3H$. We experimented here the use of the two different forcing terms described before.

### 3.2.1 Constant Pressure Gradient

In this part we are going to analyze the DNS' with the CPG forcing term. The validation was made with Figure 2 of the Chan-Braun et al. [8] study, thanks to the online plot digitizer [31]. We imposed in this case $Re_\tau = 183$, that happens to be the value found by the authors from their CFR code after imposing the correct $Re_b$. This could be a problem, because it will introduce some error in the results due to the difference in the Reynolds numbers we will have. As previously done we used two different grid-size and the same average method.

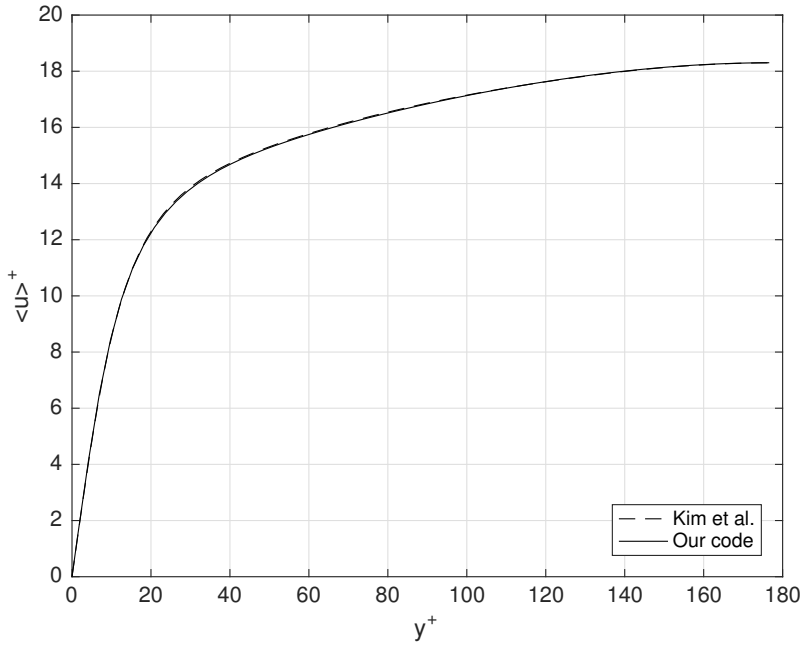


Figure 3.2: Comparison of the mean velocity over horizontal planes in the homogenous direction and time with the y grid-size of Kim et al.[14] for channel flow

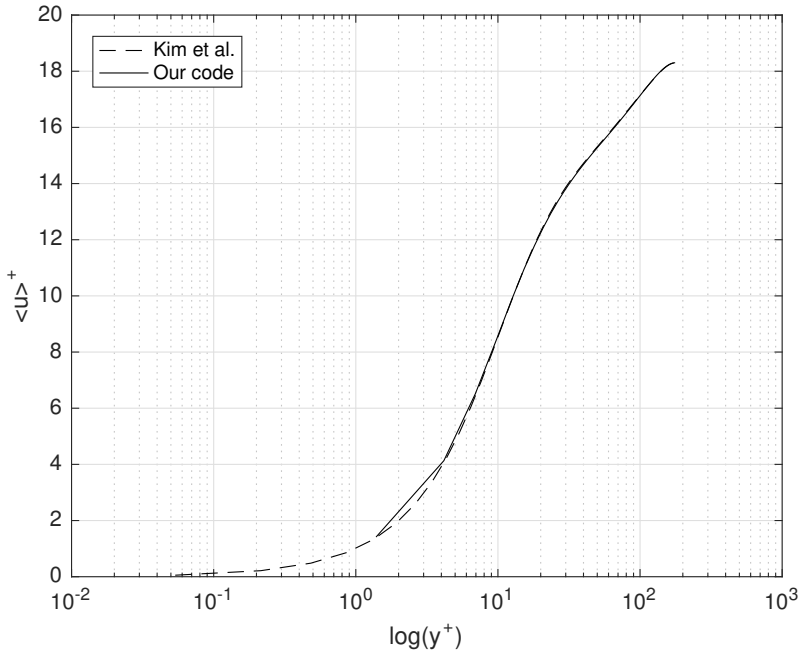


Figure 3.3: Comparison of the mean velocity over horizontal planes in the homogenous direction and time with the y grid-size of Kim et al. [14] with semilogarithmic axes for channel flow

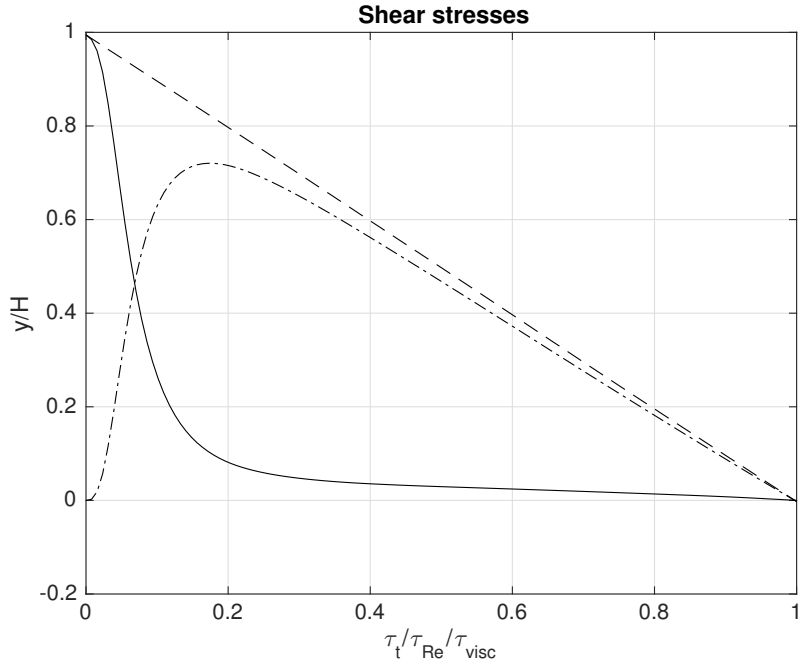


Figure 3.4: Shear stresses non-dimensionalized by $Re_\tau$ with double of the y grid-size of Kim et al. [14] for channel flow

**coarser grid** First we developed the initial conditions with a coarser grid-size in order to save some computational time. In this case we have a grid with the following size 1536 x 128 x 384; in Chan-Braun et al. [8] study the authors used a uniform grid-size as we did. We chose to use 11.4 time units to make the average.

**finer grid-size** Once we had the results we used the previous computation with a coarser grid as initial condition for the Chan-Braun et al. [8] grid-size: the grid points were doubled in every direction. The only variable different from the previous computation is the grid-size, that now is 3072 x 256 x 768. This should give us better results than the previous computation, because we are using exactly the same parameters used by the authors of the paper, exept for the forcing term of course.

### Comparison

In this section we compare the results of our code to the ones of Chan-Braun et al. [8] for the two grid-sizes defined above.

**coarser grid-size** Thanks to Figure 3.7 it is possible to noticed how our code underestimated the value of the velocity on the center-line; this is a major difference, because the underlines a strong dissimilarity in the two flows and, consequentely, the friction coefficients will be different; it was impossible to compute this values because in the data from Chan-Braun et al. [8] study $\tau_w$ was not present. We could have used the value of $\langle uv \rangle$, but

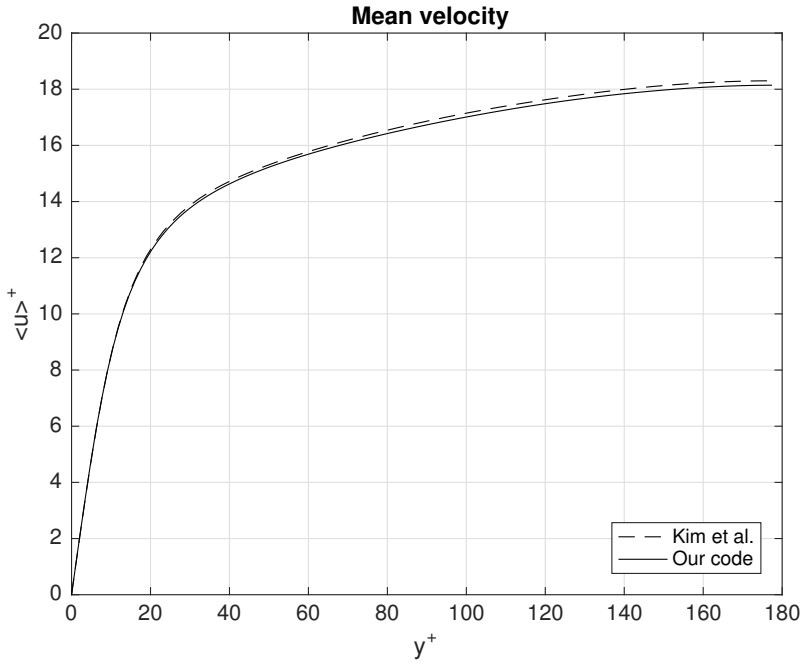


Figure 3.5: Comparison of the mean velocity over horizontal planes in the homogenous direction and time with double of the y grid-size of Kim et al. [14] for channel flow

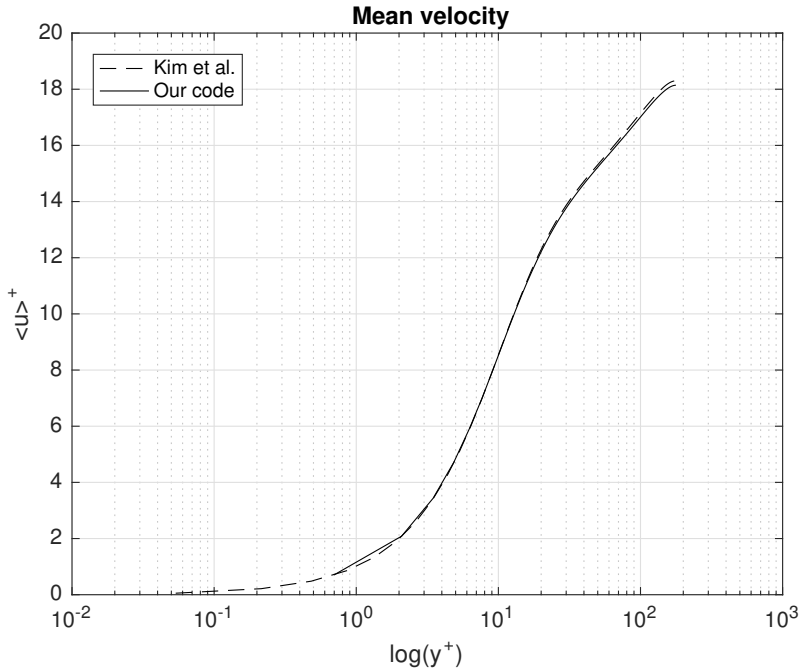


Figure 3.6: Comparison of the mean velocity over horizontal planes in the homogenous direction and time with double of the y grid-size ofKim et al. [14] with semilgarithmic axes for channel flow

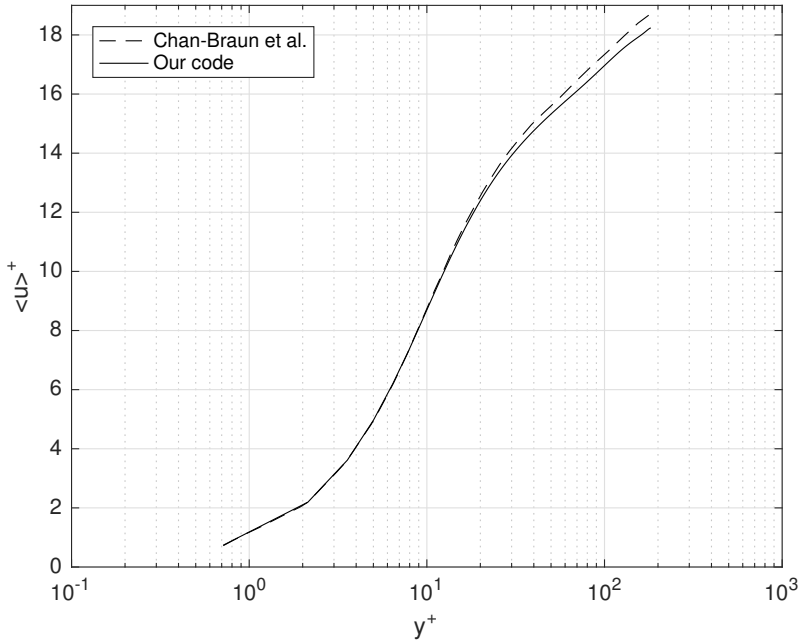


Figure 3.7: Comparison of the mean velocity over horizontal planes in the homogenous direction and time with half of the y grid-size of Chan-Braun et al. [8] with semilgarithmic axes for open channel (CPG)

its values were available only for the rough case and not for the smooth one we are considering. The error is probably due to the fact that we are using a different $Re_\tau$, in fact computing $Re_b$ from our computation, thanks to Equation 2.10, we found a difference of more than 1% from the value imposed in the paper[1]. It is important to notice that the grid-size is the same as can be seen in Figure 3.7.

**finer grid-size** Figure 3.8 shows that in this case we found a bigger difference than in the previous one: computing the $Re_b$ we found that the dissimilarity is close to 1.2%. This is probably due to the fact that this time the grid-size is the one used in the rough case and changing another parameter (grid-size) could not make our results closer to the paper's ones. Anyway, we considered this validation convincing enough to go on and add the rough-wall bottom to the open channel flow.

### 3.2.2 Constant Flow Rate

The code is capable to use the CFR strategy as forcing term; this time the comparison was made with the Figure 2 of Chan-Braun et al. [8] paper using

[1] As written before, in Chan-Braun et al. [8] study the authors used CFR, while we used CPG: we imposed $Re_\tau$ and found $Re_b$, while they did the opposite

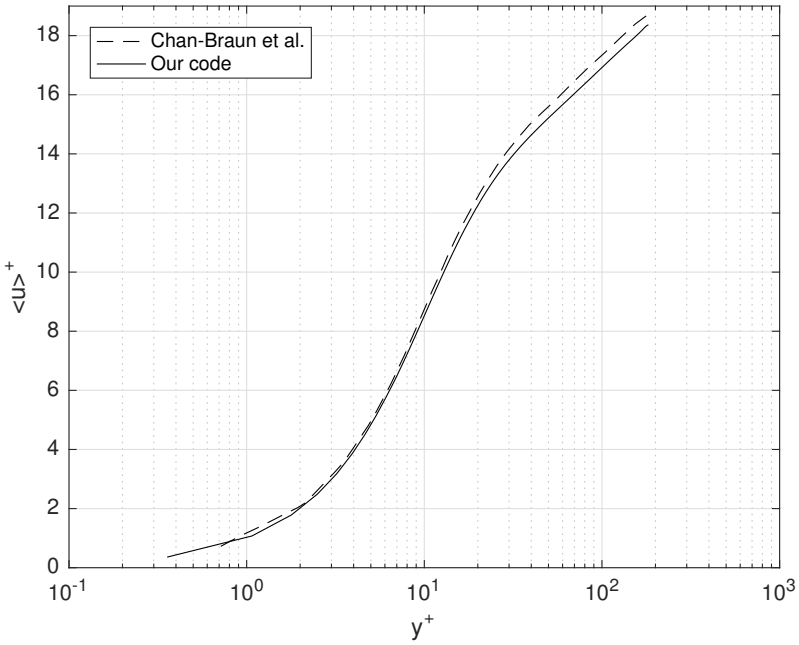


Figure 3.8: Comparison of the mean velocity over horizontal planes in the homogenous direction and time with the y grid-size of Chan-Braun et al. [8] with semilogarithmic axes for open channel flow (CPG)

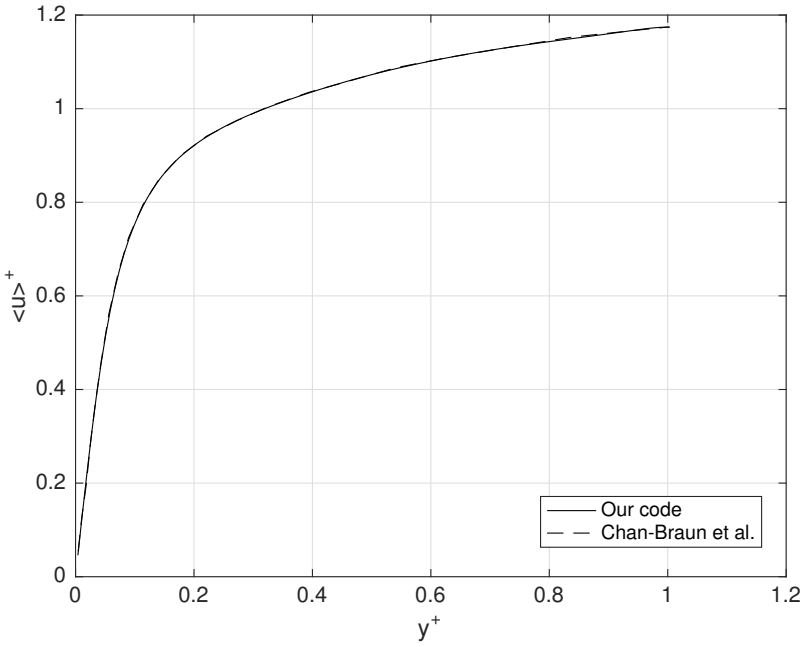


Figure 3.9: Comparison of the mean velocity over horizontal planes in the homogenous direction and time with half of the y grid-size of Chan-Braun et al. [8] for open channel (CFR)

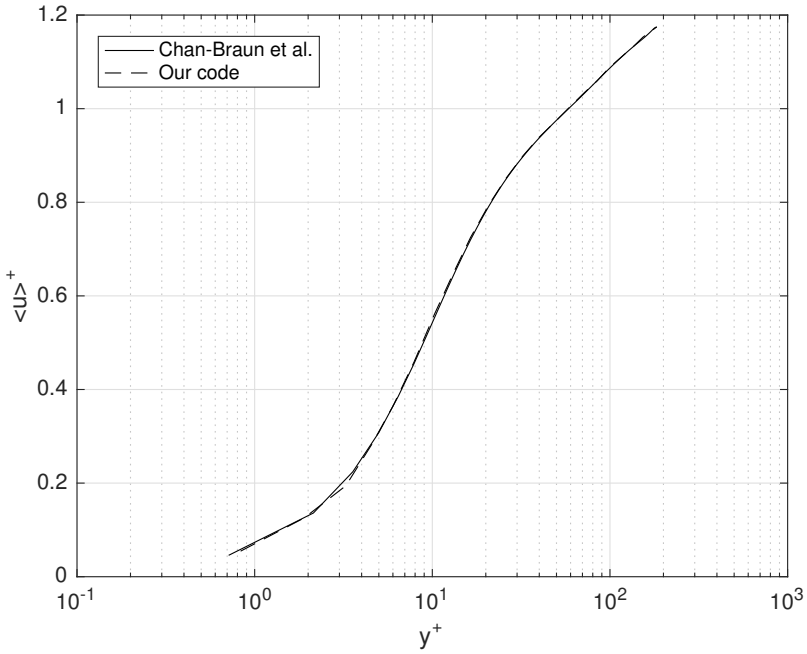


Figure 3.10: Comparison of the mean velocity over horizontal planes in the homogenous direction and time with half of the y grid-size of Chan-Braun et al. [8] with semilgarithmic axes for open channel (CFR)

the plot digitizer [31] to get the data. This method of course introduced some error, but the values found from our code were very close to the ones digitized. In order to have the same results we chose $Re_b = 2870$, as in the paper, and after the computation, we got $Re_\tau$ in the post-processing thanks to Equation 2.23. The domain size and the grid-size are as the same as the ones of the coarser computation. The time units for the average are 200 because of the different scaling of the velocity: this time we have $\frac{\overline{u}}{U_b}$, which is almost fifteen times smaller than $\frac{\overline{u}}{u_\tau}$, result of the CPG computation.

**Comparison**

In this section we compare the results we had with the ones digitized from the paper: Figure 3.9 shows the mean velocity as a function of the distance from the wall, while Figure 3.10 shows the same data but in logarithmic axis (in this way it is easier to see the differences between the two curves). It is clear from this figures that using the same forcing term of Chan-Braun et al. [8] study we had an enourmously smaller difference than with the CPG case: the difference on the $U_b$ we found is 0.1% and we considered this results much better than the one found with the other forcing term. This made us understand that the differences we had were due to the different forcing strategy and they were not part of our code, they were probably due to the fact that we used a different Reynolds number and these difference reflected on the results. Unfortunately the CFR forcing term was not perfectly working for the sphere case, so the future are probably due to the use of a different Reynolds number.
Moreover we have to consider that the values of Figure 3.9 and Figure 3.10 are the actual values we digitized from Figure 2 of Chan-Braun et al. [8] study, while we had to convert them in order to make the comparison with our code in Figure 3.7 and Figure 3.8. With convert the author means from the $U_b$-non-dimensionalization to the $u_\tau$ one. This could have added more errors to the comparison with the data from the paper.

# Chapter 4

# Channel flow with roughness

This validation is the most complicated, but also the most important one. In the following Chapter we are going to present the details of the computation and a comparison between the smooth case and the rough case in which we want to find the behaviour previously presented (underlined in Figure 1.2).

## 4.1 Description of the geometry

To simulate a rough wall we added a layer of spheres on the bottom of the channel and a layer under the wall at a distance of $\frac{D}{2} - \sqrt{2}\left(\frac{D}{2} + \delta x\right)$; the latter have the function to fill the gap between the upper-layer spheres and, in the rest of this thesis, they will be called caps. The distance in $x$- and $z$-directions between two sphere is $2\delta x$. The geometry is shown in Figure 4.1; this is the geometry defined in Chan-Braun et al. [8] study.
As previously done in the case of the smooth open channel flow we compute a coarser grid-size to develop the turbulence and then we computed the desired grid-size starting from this result. The two computations are described in the following part. Furthermore we considered the flow is considered statistically stable and the average appropriate once the total shear stress over the sphere layer was linear.
In Chan-Braun et al. [8] paper, in order to scale the results, two quantities were defined:

$y_0 = 0.8\,D$ is a fictitious position of the wall, because on the rough bottom it cannot be unambiguously defined. The explanation of this choice can be found in the Appendix of the Chan-Braun et al. [8] study.

$u_\tau$ this value was extrapolated from the value of the total shear stress above the sphere down to $y_0$. It is easy to understand that this decision makes the value of $u_\tau$ completely arbitrary and, consequently, we had to adopt this technique to compare our results with the paper.

This two values defines $Re_\tau$, it follows that, accepting our code $Re_\tau$ at the wall as input, we had to link the value given in the paper and our definition as

follows:

$$Re_\tau = \frac{u_\tau H}{\nu} = \frac{u_\tau h}{\nu}\frac{H}{h} = (Re_\tau)_{Uhlmann}\frac{H}{h} \quad \wedge \quad h = H - y_0 \tag{4.1}$$

finding in the end $Re_\tau \simeq 197$. It is important to underline that this value changes with $y_0$ that depends on the diameter of the sphere, so we will have a different $Re_\tau$ if we choose to change the diameter of the spheres.
In order to avoid to take into count of the velocity inside the spheres in the average process, we decided to impose a velocity of $-1000$ inside them and use an *IF* to skip this values during the computation of $\langle u \rangle$.
It is easy to notice how the smooth cases were reproduced quite well, while adding the spheres gave us results with slight differences respect to the paper case. This was due to the fact that in the paper chosen to make the validation [8] the authors used a different strategy for the forcing term: in the paper they imposed $Re_b$ in their code and they computed $Re_\tau$, while our code was based on $Re_\tau$ and we were able to compute $Re_b$ at the end (with Equation 2.10). This make a huge difference in the two computation because the two forcing term should develop the same turbulent flow theoretically (statistically speaking), but, as underlined in Quadrio et al. [30] study, they lead to different fluctuations of quantities: CPG will lead to a fluctuating flow rate in time, while with CFR we will have a temporally fluctuating pressure gradient. These fluctuations depends on the DNS characteristics and they become smaller for larger domains, but are always present in a domain of finite size, then in every numerical simulation. In the same paper is shown that for CPG there are no errors in the value of the friction Reynolds number (the small difference is due only to the time-avereaging process), while underlines small errors in the non-CPG simulations. In Chan-Braun et al. [8] the value of $Re_\tau$ was given, but it was scaled on a completely arbitrary origin $y_0$ and it was not possible to use directly this value for our computation. As previously underlined it has been impossible to use the same forcing term adopted by Chan-Braun et al. [8], because of the error on the constant flow rate we have in our code with the CFR forcing term.

**Coarser grid** in order to avoid the transient time to reach the statistically stable state in the finer case, we got the results from the computation on a coarser mesh and then we extrapolate the velocity and pressure fields in order to impose them as initial conditions in the finer one.
We have a grid-size of $1536 \times 128 \times 768$. We chose to average over 10 time units.

**Finer grid-size** Once we had the results from the coarser case we was able to reproduce the Chan-Braun et al. [8] case, in which the grid-size is $3072 \times 256 \times 1536$. This time we used 12.8 time units for the average.

## 4.2 Comparison

In this section we are going to show the results we had from our code for the rough wall case for the two grid-sizes.

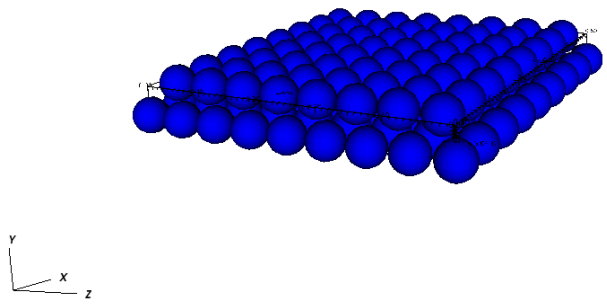


Figure 4.1: 1 x 1 domain with the distribution of spheres

In order to define the accuracy of our code we decided to use two quantities: the bulk velocity and the friction Reynolds number. For the former we used its definition, we had the mean velocity from the code and we computed the integral thanks to the Matlab command `trapz`. The other comparison we made was with $Re_\tau$, because of the approximation we made with Equation 4.1. In order to compare the value of the friction Reynolds number we had to compute the value of it in the position $y_0$ (as made by Chan-Braun et al. [8]):

$$Re_\tau = \frac{u_\tau H}{\nu} \tag{4.2}$$

We also know that:

$$u_\tau = \sqrt{\frac{\tau_w}{\rho}} = 1 \tag{4.3}$$

because $\rho$ and $\tau_w$ are already non-dimensionalized. Knowing this we can write:

$$Re_\tau = \frac{u_\tau H}{\nu} = \frac{H}{\nu} \tag{4.4}$$

It is easy to see that to find the friction Reynolds number in $y_0$ we have only to multiply $Re_\tau$ times $u_\tau\big|_{y_0} = \sqrt{\tau(y_0)}$. We obtain in the end:

$$Re_\tau\big|_{y_0} = \frac{u_\tau\big|_{y_0} H}{\nu} = \frac{\sqrt{\tau(y_0)}H}{\nu} = Re_\tau\sqrt{\tau(y_0)} \tag{4.5}$$

Once we extrapolated the value of $\tau(y_0)$ from our code output, it was possible to compare our friction Reynolds numbers with the one of Chan-Braun et al. [8]. An additional comparison was possible here, thanks to the Reynolds stresses data found online at [35]. This comparison is very important because the peak of $uu$ is also the peak of the turbulence production and, studying the difference between our code position and the one of the paper we can really consider the

differences between the two, avoiding the comparison of the friction Reynolds number.

**coarser grid-size** Figure 4.2 and Figure 4.3 show the comparison between the mean velocity profile of the paper and the discrete data (interpolated) computed by our code in normal and semilgarithmic axes respectevely. From this outputs we have been able to find the bulk velocity and compare it to the one computed in the paper thanks to Equation 2.6. We found a difference of 2.1% on $U_b$ that we considered satisfactory, because the friction Reynolds number we found overestimated the one of the paper of 3%. This is due to the approximation we had to impose, because we used a different forcing term (CPG), as previously explained. Considering the results we had on the smooth wall case, it would have been better to use the CFR forcing term, but we did not develop it for the sphere case, because of the errors we found on the flow rate, that we considered inadmissible.

Figure 4.4 show the Reynolds stresses; the position for the $uu$ peak in Chan-Braun et al. [8] study is $15.2\,y^+$, while in our code is $16.78\,y^+$. This difference is probably due to the grid-size, because in this case it is much more important than in the previous ones. The reason why the grid-size is more important now is that the distance between two spheres in the paper is $2\delta x$, but we have half of the grid points in $x$ and $z$, so our distance will be $\delta x$; because of that the part of the flow between the spheres is more approximated and the computation with the IBM will give us much worse results. In fact we have a difference of 10% on the peak position. We expect anyway this value to decrease once we will use the same grid-size.

**finer grid-size** In this case we reproduced exactly the study of Chan-Braun et al. [8].

These are the results: Figure 4.5 and Figure 4.6 show the comparison between the mean velocity profile of the paper and the discrete data (interpolated) computed by our code in normal and semilgarithmic axes, respectevely. Computing the bulk velocity from them we found a difference of 2% and this can be seen as a confirmation of our previous hypothesis: if the difference was due to the grid-size, increasing it the difference would decrease, while in this case it remains almost the same. Same old same old for the friction Reynolds number for which we found a difference of 3%. These values confirm that they are due to the approximation of the Reynolds number at the wall and, consequentely, to the different forcing term we used. We could have probably changed the Reynolds number to go closer to the paper results with a trial and error method, but we preferred to use a theoretical method (the one described with Equation 4.1), because it is justifiable from a mathematical point of view.

Figure 4.7 shows the Reynolds stresses. We should find now a smaller difference than the previous one. The peak in this case was $16\,y^+$ and the difference respect to the paper value is smaller than the one we found before; we have a 5% of difference to compare with the 10% we had before. In this case we confirmed that the grid-size is very important in the case with the spheres, or rather the IBM.

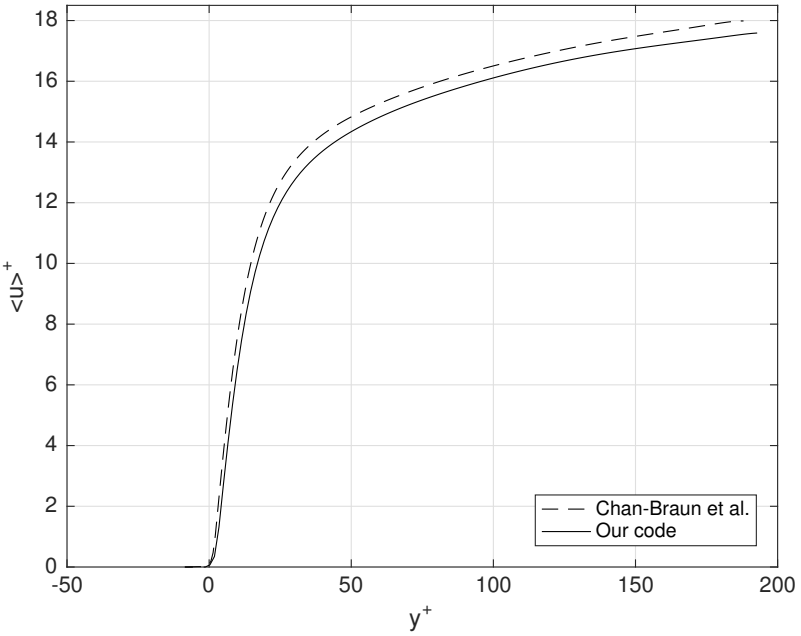


Figure 4.2: Comparison of the mean velocity over horizontal planes in the homogenous direction and time with one eight of the grid-size of Chan-Braun et al. [8] for an open channel flow over a rough wall

It is easy to notice how adding the spheres, so the IBM, gave us worse results than the previous ones; this can be explained in different ways. As previously underlined, using a different forcing term made a slight difference in the results, because the Reynolds numbers were different in our code and in Chan-Braun et al. [8]. This is why we decided to use this quantity and $U_b$ to estimate the errors of our code. Moreover the complexity of the flow is higher than in the previous cases and the results are much more sensitive to small changes in the initial conditions. It is anyway a small difference and the values we found are very close to the paper's ones, we can then consider the validation satisfactory.

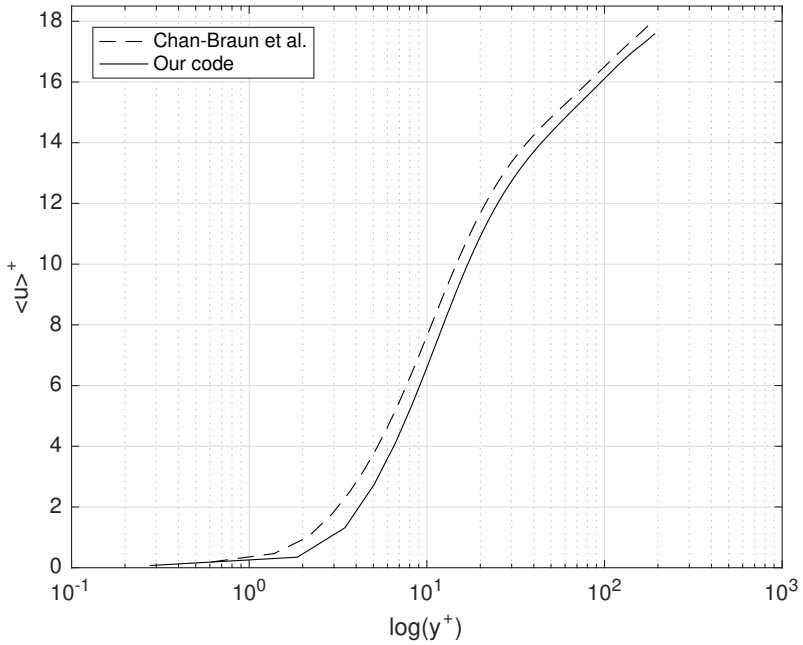


Figure 4.3: Comparison of the mean velocity over horizontal planes in the homogenous direction and time with one eight of the grid-size of Chan-Braun et al. [8] with semilogarithmic axes for an open channel flow over a rough wall

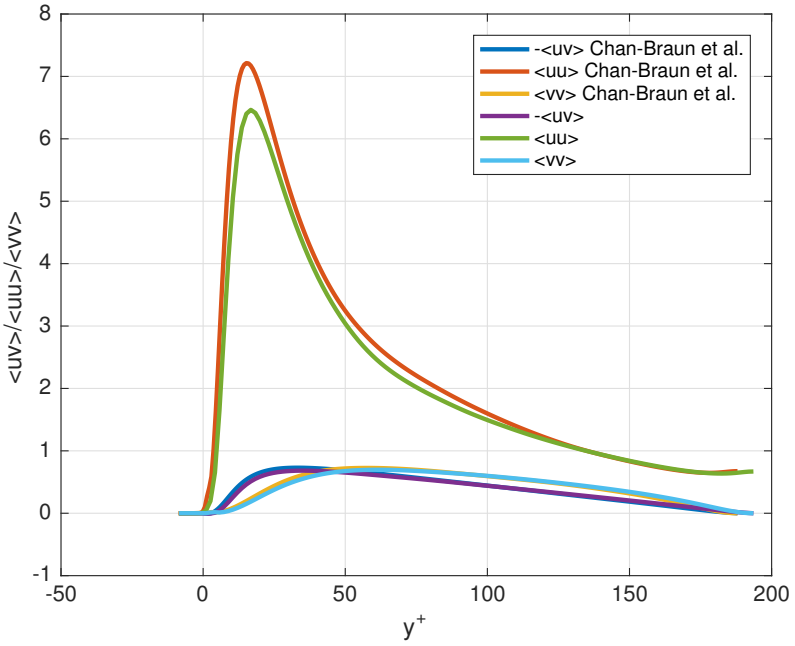


Figure 4.4: Comparison of the first three components of the Reynolds stresses with one eight of the grid-size of Chan-Braun et al. [8]

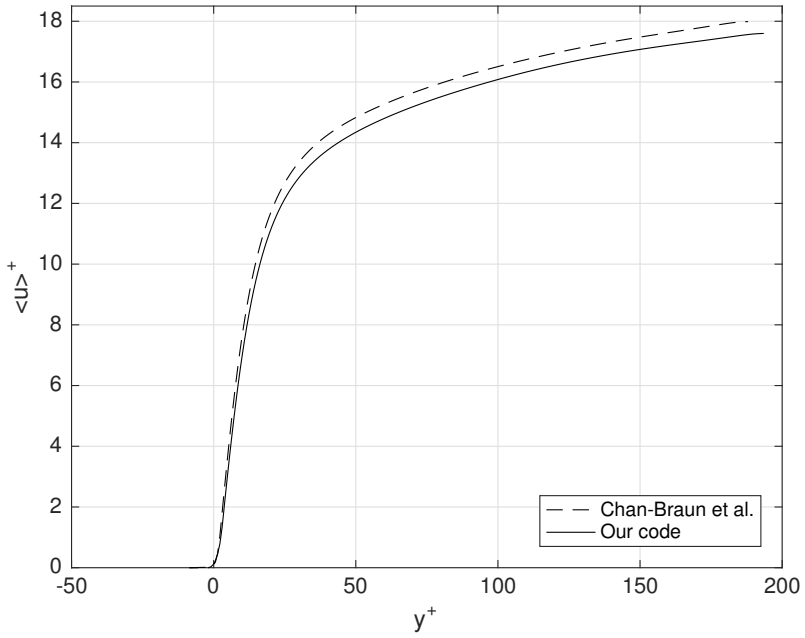


Figure 4.5: Comparison of the mean velocity over horizontal planes in the homogenous direction and time with the grid-size of Chan-Braun et al. [8] for an open channel flow over a rough wall

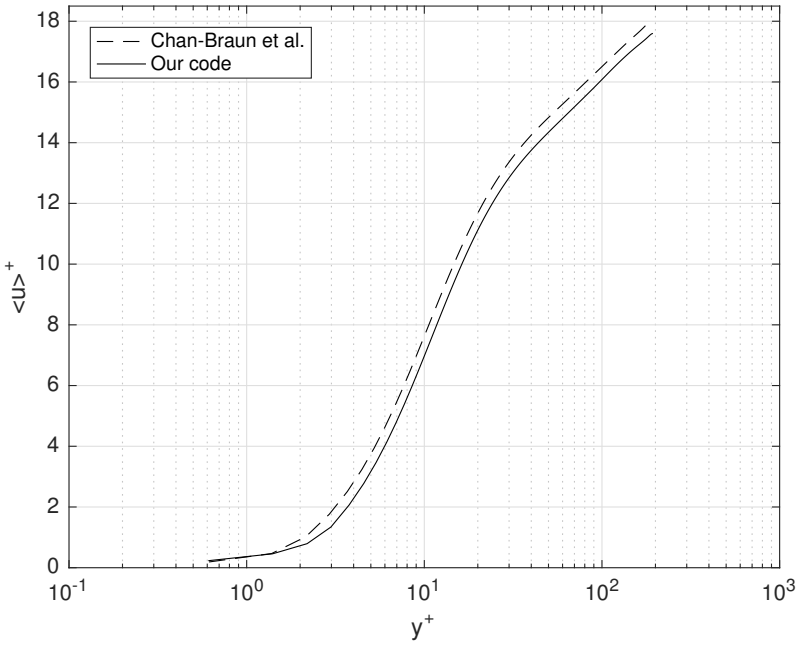


Figure 4.6: Comparison of the mean velocity over horizontal planes in the homogenous direction and time with the grid-size of Chan-Braun et al. [8] with semilogarithmic axes for an open channel flow over a rough wall

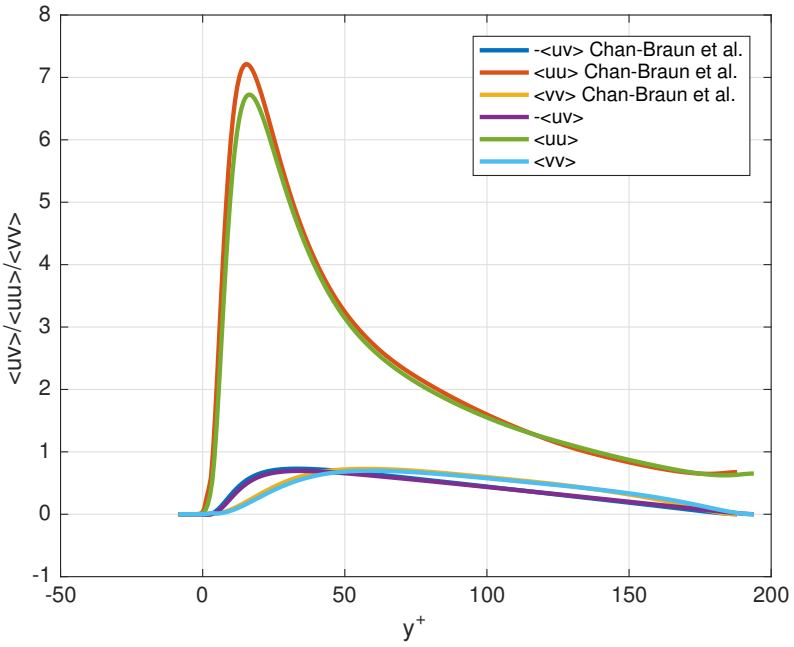


Figure 4.7: Comparison of the first three components of the Reynolds stresses with the grid-size of Chan-Braun et al. [8]

## 4.3 Law of the wall

In the following section we are going to compare the results of our DNS with the equations defining the theoretical behaviour of $u^+$ defined in the first Chapter. Moreover, we will focus our attention on the differences between a turbulent flow over a smooth and a rough wall to define which precision our code reaches. As can be seen in Figure 4.8, the theoretical curves described by Equation 1.8 and Equation 1.9 (with $\kappa = 0.4$ and $B = 5.5$) fit quite well with the smooth simulation made by our code. It is also clear from the same Figure the presence of the difference in the viscous velocity $\Delta u^+$ underlined in the first Chapter. In order to find the theoretical curve for the rough case we applied the logarithmic law, but this time the constant is different, because of the presence of the rough wall. We are not in the case of a fully rough surface, because the ratio between the dimension of the roughness (in our case $d = 14\delta x$) and the viscous lengthscale ($\delta_\nu$) is:

$$d = 0.0547 \tag{4.6}$$

$$\delta_\nu = 0.00508 \tag{4.7}$$

$$\frac{d}{\delta_\nu} \simeq 10 \tag{4.8}$$

In this case, the theoretical logarithmic curve reads:

$$u^+ = \frac{1}{\kappa} ln\left(\frac{y}{s}\right) + B_2 = \frac{1}{\kappa} ln(y^+) + \frac{1}{\kappa} ln(d^+) + B_2 \tag{4.9}$$

where $B_2 = 10$ from the Nikuradse [23] data. As previously underlined the result we have for the smooth wall is better than the one we have for the rough case. This is probably due to the greater complexity that the IBM add to the code.
It is possible to notice in Figure 4.9 that the difference between the two cases are almost the same[1]. Having the $y^+$ data a different arrangement in the rough and the smooth cases it was impossible to directly find the difference between the values of $u^+$ in the two configuration. We decided then to integrate between the same $y^+$ the two curves and find the difference between them, then divide them with $y^+$ in order to have something similar to $\Delta u^+$. We considered:

$$\Delta u^+ = \frac{1}{y_s^+} \int_0^{y_s^+} u_s^+ dy - \frac{1}{y_r^+} \int_0^{y_r^+} u_r^+ dy \tag{4.10}$$

where $\cdot_s$ is the result with the smooth wall, while $\cdot_r$ with the rough one. This difference is due to the fact that the friction Reynolds number is different in the two cases, because the addition of the spheres increase this value in the computation made by Chan-Braun [8]: using a CFR strategy they imposed the same bulk Reynolds number in every computation, but, because of that, they found different friction Reynolds numbers for every case. On the contrary our computation is based on $Re_\tau$ and we had to impose their values in order to have a validation, trying to find the same $Re_b$ they used as a result. This solution

[1] The reason why in the Chan-Braun et al. [8] data there are less points close to the wall in the smooth case is that those data were digitized from a figure of the paper and they were not available online

| | Chan-Braun et al. [8] | our code | $\delta(\Delta u^+)$ |
|---|---|---|---|
| $\Delta u^+$ | 0.98 | 1.01 | $\simeq 3\%$ |

Table 4.1: Comparison between the difference in the viscous velocity due to the roughness found by Chan-Braun et al [8] and our code

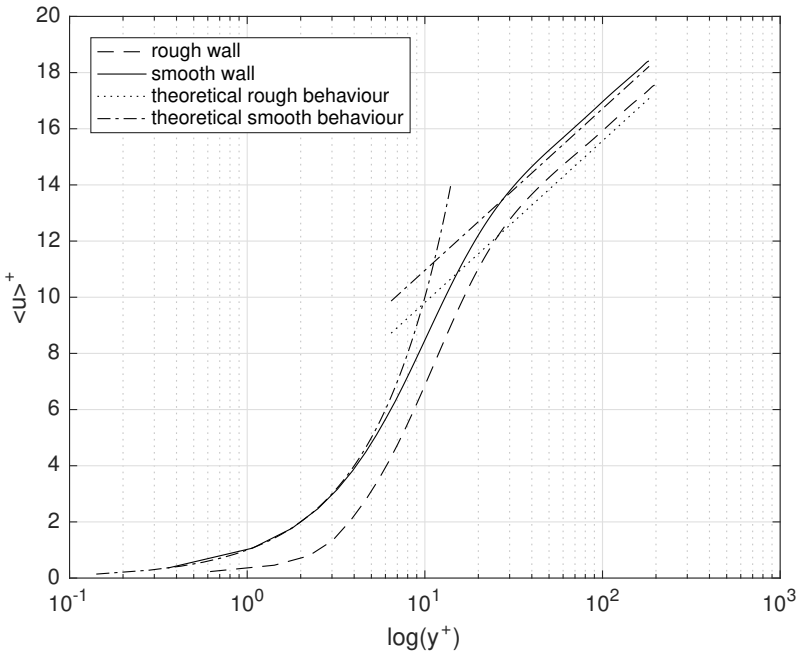


Figure 4.8: Comparison between rough and smooth wall theoretical curves and the results of our DNS

made the computation of the difference in the two cases harder: the axes are shifted because of the different values of $Re_\tau$ that define $y^+$.
We found the values in Table 4.1. We considered the difference with Chan-Braun et al. [8] quite small and th validation satisfactory. It is important to underline again that the data for the DNS with the smooth wall made by Chan-Braun et al. [8] were digitized and this move could have introduced some error itself. Therefore, the value found for the error must be considered very carefully and only a qualitative comparison is possible. From Figure 4.10[2] it is possible to notice that the value of 1 is in the correct range for $k_\infty^+ \simeq 10$.

[2]In this case the Figure was taken from Chan-Braun et al. [8] and it was considered useless to exchange $\Delta U^+$ with $\Delta u^+$ always used in this thesis.

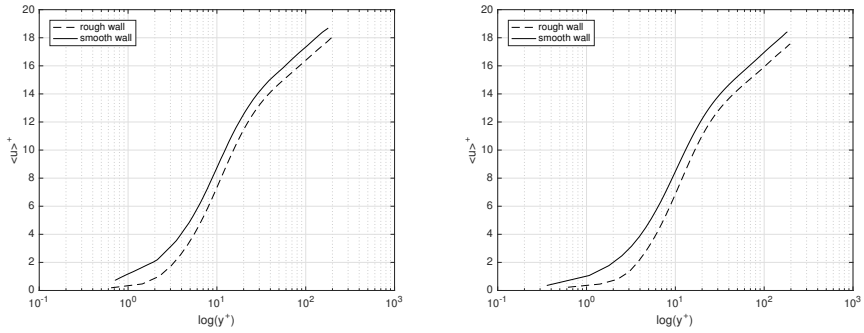


(a) *Chan-Braun et al. [8].* (b) *Our code.*

Figure 4.9: Comparison between the results we have from our code and the ones found by Chan-Braun et al [8]

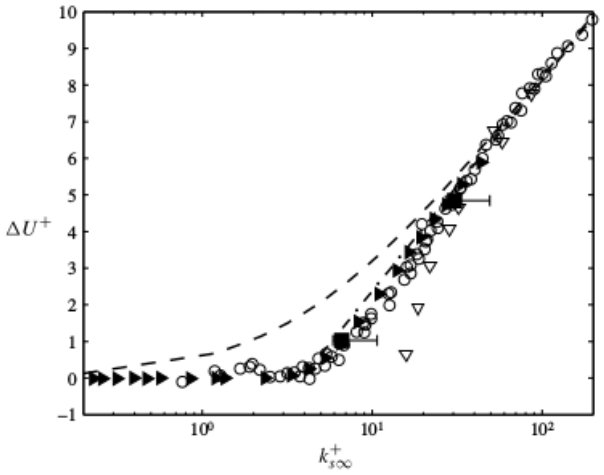


Figure 4.10: Roughness function for several transitionally rough surface as a function of the Reynolds number based on $k_\infty^+$ from several paper. Picture taken from Chan-Braun et al. [8].

# Chapter 5

# Conclusions and future work

We can assure from the previous Chapters that the code is able to reproduce the theoretical prediction of the logarithmic law and the main statistics behaviour of a turbulent channel flow.
In the rough case we had a worse validation with the study of Chan-Braun et al. [8] than in the smooth case and this was probably due to the approximations and complexity introduced by the IBM. Moreover, the differences found respect to Chan-Braun et al. [8] paper is partially due to the difficult comparison between the two different forcing term strategies used. An extension of our code could be the addition of the possibility to use the CFR forcing term for the rough wall case, that could make the code results easier to be compared with other studies. In fact, thanks to a faster transient, CFR is usually the most adopted forcing term for the DNS of a turbulent channel flow. Therefore this solution could improve the speed of the post-processing, avoiding annoying conversions of data and input. Moreover, an extension like the one described above could allow to understand why the code gave us an error in the flow rate. This can be a symptom of a small problem in some part of it that can be solved thanks to this additional study. Additionally it would not be very complicated to do add this extension, because the code is already working and the only thing to do would be a debug.
The study presented is the first step for the future project underlined in the first Chapter, in which the DNS team of UCI will add another transport and diffusion equation to the code in order to compute the paths of the contaminants particles movement. This is a very interesting field that has not studied yet and could have a very important impact on the future of the research on pollution and containation of water. In the few time I was at UCI it was impossible to completely finish the project, but I am sure that in the future they will be able to solve the problems found and create a fast code able to simulate those kind of flows.

# Appendix

## A.1 Initial Conditions

At the beginning a lot of problems were found in choosing the right initial conditions to reach a statistically stable turbulent channel flow. With a divergence-free sinusoidal perturbation of the Poiseuille solution, after a while, the flow returned laminar. The correct initial conditions was found thanks to the Ph.D. dissertation of [10]. These initial conditions are found trying to mimic the behaviour of a turbulent flow close to the bottom wall; keeping the values of the constants defined in the paper and using a parabolic behaviour as basic velocity profile (at which we added the paper perturbation) it was possible to reach the turbulent statistically steady state. The peak of the parabola was chosen trying to minimize the transient time. Here the definition of the three perturbation velocities:

$$\begin{cases} u(x,y,z) = \dfrac{A}{2}\cos(B\,z)\dfrac{y}{30}e^{-Cy^2+\frac{1}{2}} \\ v(x,y,z) = 0 \\ w(x,y,z) = D\sin(E\,x)y\,e^{-F\,y^2} \end{cases} \tag{A.1}$$

where we chose:

$$\begin{cases} A = 10 \\ B = 3 \\ C = 0.1 \\ D = 10 \\ E = 5 \\ F = 0,1 \end{cases} \tag{A.2}$$

in order to have the fastest transient.
With the Constant Flow Rate forcing term the initial conditions had to be adjusted, being the velocity non-dimensionalized by $U_b$, instead of $u_\tau$ (we know that $U_b > u_\tau$): the initial conditions have been scaled consequently.

## A.2 Post Processing

The output of the code gives a *.txt* file every *nout* (defined in the input file) with six columns:

**y grid-points**

**mean shear stress** Starting from its definition:

$$\tau = \rho\nu\frac{d\langle u\rangle}{dy} - \rho\langle u'v'\rangle = \frac{1}{Re}\frac{d\langle u\rangle}{dy} - \langle u'v'\rangle \tag{A.3}$$

Using a first order approximation to compute the derivative term, Equation A.3 becomes:

$$\tau(j) = \frac{1}{Re}\frac{\langle u_j\rangle - \langle u_{j-1}\rangle}{\delta y} - \langle u'v'\rangle_j \quad where \quad j = 1, gsize(2)+1 \tag{A.4}$$

where $gsize(2)$ is the last grid point in the y direction. It is obvious that, in order to compute $\tau$, it was necessary to compute $\langle u'v'\rangle$ before, from Equation A.13.
At the boundaries the value of the shear stress had to be approximated due to the boundary conditions; Equation A.4 becomes:

$$\tau(0) = \frac{1}{Re}\frac{\langle u\rangle_0 - \langle u\rangle_{-1}}{\delta y} - \langle u'v'\rangle_0 = 2\frac{\langle u_0\rangle}{\delta y} - \langle u'v'\rangle_0 = -\langle u'v'\rangle_0$$
$$\tau(gsize(2)) = \frac{1}{Re}\frac{\langle u\rangle_{gsize(2)+1} - \langle u\rangle_{gsize(2)}}{\delta x(2)} - \langle u'v'\rangle_{gsize(2)} = 0$$

because of the boundary condition at the wall:

$$\langle u\rangle_{-1} = -\langle u\rangle_0 = 0 \tag{A.5}$$

while for the Neumann boundary condition at the top of the channel:

$$\frac{d\langle u\rangle}{dy} = 0 \quad \rightarrow \quad \langle u\rangle_{gsize(2)+1} = \langle u\rangle_{gsize(2)} \tag{A.6}$$
$$\langle u'v'\rangle_{gsize(2)} = 0 \tag{A.7}$$

From these equations the averaged shear stress was found directly, because $\langle u\rangle$ is the mean velocity (the average process on this quantity will be described in the following part)

**mean velocity** This quantity was found as follows:

$$\langle u\rangle_j = \frac{\sum_{i=0}^{gsize(1)}\sum_{k=0}^{gsize(3)} u_j(i,k)}{gsize(3)\,gsize(1)} \quad \wedge \quad j = 0, gsize(2) \tag{A.8}$$

**reynolds stresses** For all of the Reynolds stresses the same computation was applied, in the following passages.
First of all the turbulent components of the velocity must be found:

$$u' = u - \langle u\rangle \tag{A.9}$$
$$v' = v \tag{A.10}$$

Then a second order approximation was used to compute the total Reynolds

stresses for every slice as:

$$\langle u'u' \rangle_j^{total} = \sum_{i=0}^{gsize(1)} \sum_{k=0}^{gsize(3)} \frac{(u'_{j+1}(i,k) + u'_j(i,k))^2}{4}$$

$$\langle v'v' \rangle_j^{total} = \sum_{i=0}^{gsize(1)} \sum_{k=0}^{gsize(3)} \frac{(v'_j(i+1,k) + v'_j(i,k))^2}{4}$$

$$\langle u'v' \rangle_j^{total} =$$

$$= \sum_{i=0}^{gsize(1)} \sum_{k=0}^{gsize(3)} \frac{(v'_j(i+1,k) + v'_j(i,k))(u'_{j+1}(i,k) + u'_j(i,k))}{4}$$

In the end:

$$\langle u'u' \rangle_j = \frac{\langle u'u' \rangle_j^{total}}{gsize(3)\, gsize(1)} \tag{A.11}$$

$$\langle v'v' \rangle_j = \frac{\langle v'v' \rangle_j^{total}}{gsize(3)\, gsize(1)} \tag{A.12}$$

$$\langle u'v' \rangle_j = \frac{\langle u'v' \rangle_j^{total}}{gsize(3)\, gsize(1)} \tag{A.13}$$

# Bibliography


[1] D. W. Bechert, M. Bruse, W. Hage, G. T. Van Der Hoeven, and G. Hoppe. Experiments on drag-reducing surfaces and their optimization with an adjustable geometry. *J. Fluid Mech.*, 338:59–87, 1997.

[2] D. M. Birch and J. F. Morrison. Similarity of the streamwise velocity component in very-rough-wall channel flow. *J. Fluid Mech.*, 668:174–201, 2011.

[3] S. Bisceglia, R. J. Smalley, L. Djenidi, and R. A. Antonia. Structure of rough wall turbulent boundary layers at relatively high reynolds number. *14th Australasian Fluid Mechanics Conference, Adelaide University, Australia*, pages 195–198, 2001.

[4] J. P. Bons. $s_t$ and $c_f$ augmentation for real turbine roughness with elevated freestream turbulence. *J. Turbomach*, 124:632–644, 2002.

[5] A. Busse, M. Lützner, and N. D. Sandham. Direct numerical simulation of turbulent flow over a rough surface based on a surface scan. *Computers and Fluids*, 116:129–147, 2015.

[6] J. Cardillo, Y. Chen, G. Araya, J. Newman, K. Jansen, and L. Castillo. Dns of a turbulent boundary layer with surface roughness. *J. Fluid Mech.*, 729:603–637, 2013.

[7] P. Castro. Rough-wall boundary layers: mean flow universality. *J. Fluid Mech.*, 585:469–485, 2007.

[8] C. Chan-Braun, M. García-Villalba, and M. Uhlmann. Force and torque acting on particles in a transitionally rough open-channel flow. *J. Fluid Mech.*, 684:441–474, 2011.

[9] J. Claus, O. Coceal, T. Glyn Thomas, S. Branford, S. E. Belcher, and Ian P. Castro. Wind-direction effects on urban-type flows. *Boundary-Layer Meteorology*, page 1, 2011.

[10] E. de Villiers. The potential of large eddy simulation for the modeling of wall bounded flows. *Phd dissertation, Imperial College of Science, London*, 2006.

[11] L. Djenidi, R. Elavarasan, and R. A. Antonia. The turbulent boundary layer over transverse square cavities. *J. Fluid Mech.*, 395:271–294, 1999.

[12] O. Flores and J. Jiménez. Effect of wall-boundary disturbances on turbulent channel flows. *J. Fluid Mech.*, 566:357–376, 2006.

[13] A. J. Grass. Structural features of turbulent flow over smooth and rough boundaries. *J. Fluid Mech.*, 50:233–255, 1971.

[14] J. Kim, P. Moin, and R.D. Moser. Turbulence statistics in fully developed channel flow at low reynolds number. *J. Fluid Mech.*, 177:133–166, 1987.

[15] S. H. Lee and H. J. Sung. Direct numerical simulation of the turbulent boundary layer over a rod-roughened wall. *J. Fluid Mech.*, 584:125–146, 2007.

[16] S. H. Lee, H. J. Sung, and P. A. Krogstad. Direct numerical simulation of the turbulent boundary layer over a cube-roughened wall. *J. Fluid Mech.*, 669:397–431, 2011.

[17] S. Leonardi, P. Orlandi, R. J. Smalley, L. Djenidi, and Antonia R. A. Direct numerical simulations of turbulent channel flow with transverse square bars on one wall. *J. Fluid Mech.*, 491:229–238, 2003.

[18] S. Leonardi, R. J. Orlandi, L. Djenidi, and R. A. Antonia. Structure of turbulent channel flow with square bars on one wall. *J. Heat Fluid Flow*, 25:384–392, 2004.

[19] S. Leonardi, P. Orlandi, and R. A. Antonia. Properties of d- and k-type roughness in a turbulent channel flow. *Phys. Fluids*, 19:125101, 2007.

[20] F. Lucci, A. Ferrante, and S. Elghobashi. Modulation of isotropic turbulence by particles of taylor length-scale size. *J . Fluid Mech.*, 650:5–55, 2010.

[21] I. Marusic, B. J. McKeon, P. A. Monkewitz, H. M. Nagib, A. J. Smits, and K. R. Sreenivasan. Wall-bounded turbulent flows at high reynolds numbers: Recent advances and key issues. *Physic of Fluids*, 22, 2010.

[22] E. Napoli, V. Armenio, and M. De Marchis. The effect of the slope of irregularly distributed roughness elements on turbulent wall-bounded flows. *J. Fluid Mech.*, 613:385–394, 2008.

[23] J. Nikuradse. Laws of flows in rough pipes. *Tech. rep., NACA Technical Memorandum 1292*, 1950.

[24] P. Orlandi and S. Leonardi. Direct numerical simulation of three-dimensional turbulent rough channels: parameterization and flow physics. *J. Fluid Mech.*, 606:399–415, 2008.

[25] P. Orlandi, S. Leonardi, R. Tuzi, and R. Antonia. Direct numerical simulation of turbulent channel flow with wall velocity disturbances. *Phys. Fluids*, 15:3587–3601, 2003.

[26] P. Orlandi, S. Leonardi, and R. A. Antonia. Turbulent channel flow with either transverse or longitudinal roughness elements on one wall. *J. Fluid Mech.*, 561:279–305, 2006.

[27] G. Pailhas, Y. Touvet, and B. Aupoix. Effects of reynolds number and adverse pressure gradient on a turbulent boundary layer developing on a rough surface. *Journal of Turbulence*, 9:1–24, 2008.

[28] A. E. Perry, W. H. Schofield, and P. N. Joubert. Rough wall turbulent boundary layers. *J. Fluid Mech.*, 37:383–413, 1969.

[29] S. B. Pope. *Turbulent Flows*. Cambridge University Press, 2000.

[30] M. Quadrio, B. Frohnapfel, and Y. Hasegawa. Does the choice of the forcing term affect flow statistics in dns of turbulent channel flow? *P. Fluid Dyn.*, 2015.

[31] Ankit Rothagi. Webplotdigitizer. http://arohatgi.info/WebPlotDigitizer, 2017.

[32] H. Schlichting. Experimentelle untersuchungen zum rauhigkeitsproblem. *Ingenieur-Archiv*, 7:1, 1936.

[33] M. P. Schultz and K. A. Flack. The rough-wall turbulent boundary layer from the hydraulically smooth to the fully rough regime. *J. Fluid Mech.*, 580:381–405, 2007.

[34] K. M. Singh, N. D. Sandham, and J. J. R. Williams. Numerical simulation of flow over a rough bed. *J. Hydraul. Engng*, 133:386–398, 2007.

[35] Markus Uhlmann. Dns data. http://www-cfd.ifh.uni-karlsruhe.de/uhlmann/home/report.html.

[36] J. A. van Rij, B. J. Belnap, and P. M. Ligrani. Analysis and experiments on three-dimensional, irregular surface roughness. *J. Fluid Mech.*, 124: 671–677, 2002.